Biogeosciences, 23, 5571–5591, 2026
https://doi.org/10.5194/bg-23-5571-2026

Biogeosciences Open Access EGU

The Ni cycle in the Southern Ocean: insights from Ni concentrations, isotopes and metagenomics

Nolwenn Lemaitre[1,2,★], Emile Faure[3,4,5,★], Ricardo Zamora[2], Corey Archer[2], Matthias Sieber[2,6], Michael Ellwood[7], Christel Hassler[8,9], Yajuan Lin[10,11,12], Nicolas Cassar[11,12], Lois Maignien[4,13], and Derek Vance[2]

[1]LEGOS (CNRS/CNES/IRD/UT3), University of Toulouse, Toulouse, 31400, France
[2]Department of Earth and Planetary Sciences, Institute of Geochemistry and Petrology, ETH Zurich, 8092 Zurich, Switzerland
[3]Station Biologique de Roscoff, CNRS/Sorbonne University, Roscoff, 29680, France
[4]Univ Brest, CNRS, IFREMER, BEEP, Plouzané, 29280, France
[5]BRIDGE, School of Geographical Sciences, University of Bristol, Bristol, BS8 1SS, UK
[6]College of Marine Science, University of South Florida, St. Petersburg, FL 33701, USA
[7]Research School of Earth Sciences, Australian National University, Canberra, 2601, Australia
[8]Institute of Earth Sciences, University of Lausanne, 1015 Lausanne, Switzerland
[9]School of Architecture, Civil & Environmental Engineering, Alpine and Polar Environmental Research Center, EPFL, 1951 Sion, Switzerland
[10]Department of Life Sciences, Texas A&M University Corpus Christi, Corpus Christi, TX 78412, USA
[11]Division of Earth and Climate Sciences, Nicholas School of the Environment, Duke University, Durham, NC 27708, USA
[12]CNRS, Univ Brest, IRD, Ifremer, LEMAR, Plouzané, 29280, France
[13]Bay Paul Center, Marine Biological Laboratory, Woods Hole, MA 02543, USA
★These authors contributed equally to this work.

Correspondence: Nolwenn Lemaitre (nol.lemaitre@gmail.com) and Emile Faure (emile.faure@bristol.ac.uk)

Received: 18 December 2025 – Discussion started: 19 January 2026
Revised: 23 June 2026 – Accepted: 24 June 2026 – Published: 12 August 2026

Abstract. Nickel (Ni) is an essential micronutrient for marine microorganisms, involved in enzymes controlling the nitrogen cycle and metabolic responses to oxidative stress. In this study, we examine the role of potential Ni utilisation by marine microorganisms in oceanic Ni and δ^{60}Ni distributions, and specifically the influence of Ni-containing enzyme abundances on Ni isotope fractionation. Dissolved Ni concentrations and isotope compositions were measured together with microbial gene composition in Southern Ocean samples from the Antarctic Circumnavigation Expedition. We show that lower Ni concentrations are associated with higher δ^{60}Ni values in surface waters north of the Sub-Antarctic Front compared to southerly locations. The high-latitude Mertz Glacier stands as an exception, as systematics between Ni and δ^{60}Ni resemble those of low-latitude stations. No single enzyme could be identified as the sole driver of δ^{60}Ni variations across all stations, as the strength and significance of correlations varied depending on the level of precision of functional annotations and the size fractions considered. Still, relative abundances of gene clusters annotated as urease and Ni superoxide dismutase (Ni-SOD) enzymes in metagenomes correlated with δ^{60}Ni, suggesting the preferential removal of isotopically light Ni by microorganisms using these enzymes. Despite differences in enzymatic and taxonomic profiles, the three stations exhibiting heavy surface Ni isotope compositions share a specific nitrogen biogeochemistry, characterised by high particulate organic nitrogen pool and strong nitrate consumption. We thus hypothesise that Ni and δ^{60}Ni distributions reflect variations in Ni metabolic requirements driven by complex microbial and enzymatic activity linked to the relative availability of inorganic and organic nitrogen. We further propose that the use of urea as an alternative nitrogen source during the late productive season could explain the unexpected isotope fractionation observed

at Mertz. This study represents an initial exploration of the influence of enzymes and microbial communities on the Ni biogeochemical divide.

1 Introduction

The biogeochemical cycling of nutrients in the ocean is controlled by microbial organisms. Typically, nutrients are drawn down in surface waters through phytoplankton utilisation, and released at depth due to remineralisation by heterotrophic bacteria. These key biological reactions are mediated by enzymes, many of which contain transition metals (Morel et al., 2020). Among these different enzymatic roles, Ni is required as the metallocenter in "urease" enzymes that recycles urea back to bioavailable ammonia (~ 1 g atom of Ni per mol of subunit; Christians and Kaltwasser, 1986), in "NiFe hydrogenase" enzymes that oxidises dihydrogen produced during nitrogen fixation (~ 1 g atom of Ni per mol of enzyme; Cammack et al., 1994), and in "Ni superoxide dismutase" (Ni-SOD) enzymes that degrades superoxide radicals and other reactive oxygen species generated through photosynthesis and respiration (~ 0.74 g atom of Ni per mol of subunit; Youn et al., 1996; Ragsdale, 2009). Although different isoforms of the SOD enzyme are observed (including those with Mn, Fe, Cu or Zn in the metal active site), only the Ni-SOD is found in some types of cyanobacteria (*Prochlorococcus*, most *Synechococcus*, a few *Trichodesmium* species), in heterotrophic bacteria, and in the picoeukaryote *Ostreococcus* (Dupont et al., 2008b, 2010). These enzymatic roles have been evidenced by controlled culture experiments involving Ni amendments. Diatoms respond to Ni addition when grown only on urea as a nitrogen source, illustrating their utilisation of the urease enzyme, and cyanobacteria respond to Ni independently of the nitrogen source, illustrating the importance of the NiFe hydrogenase and Ni-SOD enzymes (Price and Morel, 1991; Dupont et al., 2008a, b, 2010; Egleston and Morel, 2008; Ho, 2013). These studies clearly demonstrate the essential biological role of Ni and emphasize the link between the biogeochemical cycles of Ni and nitrogen (N).

This link between both cycles may be reinforced in low-latitude oligotrophic surface waters where dissolved inorganic nitrogen is often limiting, thereby increasing the importance of alternative nitrogen sources such as urea and atmospheric dinitrogen. The acquisition of both nitrogen sources relies on the Ni-containing enzymes urease and NiFe hydrogenase, the latter protecting the nitrogen fixation process and producing energy that subsequently supports nitrogen fixation (Li et al., 2022). The Ni-SOD enzyme also plays an important role for diazotrophs as it has been shown to protect the nitrogen fixation process. Specifically, the "nitrogenase" enzyme, responsible for the dinitrogen fixation process (*nif* genes) and requiring iron as a cofactor, is vulnerable when exposed to reactive oxygen species (Chen et al., 2022). Moreover, high light conditions and oxidative stress in low-latitude surface waters may also increase Ni requirements for the utilisation of the Ni-SOD enzyme. Together, these processes could increase Ni requirements in low-latitude surface waters. Understanding microbial Ni utilisation is therefore essential to interpret global Ni distributions in the ocean.

Despite these important biological demands, Ni concentrations are never fully depleted in the surface ocean and reach a ubiquitous minimum of around $1.7\,\mathrm{nmol\,L^{-1}}$ in the surface ocean (GEOTRACES Intermediate Data Product Group, 2025). Because of this incomplete drawdown, Ni has generally not been considered as a limiting nutrient in the ocean – unlike several other bioactive trace metals that can be depleted to near zero concentrations in surface waters – and consequently Ni remains under-studied. Nevertheless, a biogeochemical divide in Ni vertical distributions has been reported between high and low-latitude oceanic regions, with surface depletion only measured at low latitudes (Sclater et al., 1976; Bruland, 1980; Middag et al., 2020). This biogeochemical divide also applies to Ni isotopes, with a significant fractionation in Ni isotopes in the surface only observed at low-latitude stations (Cameron and Vance, 2014; Takano et al., 2017; Wang et al., 2019; Archer et al., 2020; Yang et al., 2020, 2021; Lemaitre et al., 2022; Bian et al., 2024; Chiu et al., 2026). This isotope fractionation demonstrates that one or more specific processes affect Ni biogeochemistry in low-latitude surface waters. Three hypotheses have been proposed so far to explain heavier Ni isotopes in the low latitude surface ocean. The first postulates the existence of a residual non-bioavailable Ni pool complexed to organic ligands, so that the very slow dissociation kinetics of these organic complexes (Mackey et al., 2002) would limit Ni uptake by phytoplankton species. This complexed non-bioavailable Ni reservoir is expected to be isotopically heavy (Archer et al., 2020). A second hypothesis suggests that most surface-ocean Ni is bioavailable and that the $1.7\,\mathrm{nmol\,L^{-1}}$ minimum corresponds to a residual Ni pool left after macronutrient depletion in low-latitude regions. Preferential biological uptake of light Ni isotopes would explain heavy isotope compositions (John et al., 2022, 2024). A third view postulates that the biogeochemical divide between low and high latitudes could be due to specific enzymatic requirements between different ecosystems (Lemaitre et al., 2022).

In this study, we aim at testing this third proposition and whether Ni could have a special role in the microbial metabolism of low-latitude regions, where its utilisation is essential in urea acquisition, oxidative stress protection and nitrogen fixation (e.g., Price and Morel, 1991; Chen et al., 2022; Li et al., 2022). In fact, heavier surface Ni isotope compositions were found to correlate with higher nitrogen fixation rates in the North Atlantic (Lemaitre et al., 2022). However, because of the different enzymatic roles in nitrogen metabolism, disentangling the specific process (or pro-

cesses) leading to low-latitude surface water Ni depletion and isotope fractionation is challenging.

In this context, omics data appear as a promising tool to better understand the role of microbial communities and their activity in driving biogeochemical cycles (Sunagawa et al., 2015; de Vargas et al., 2015; Guidi et al., 2016; White et al., 2016). Sequenced metagenomics samples, called metagenomes, are composed of short DNA fragments (called reads) that can be assembled into longer sequences (called contigs) to recover a large fraction of the genes present in the original sampled population. The same DNA sequences can also be taxonomically and functionally annotated through comparisons with reference databases, helping to decipher the genetic potential of natural populations present in the environment (e.g., Vernette et al., 2022). Metagenomics thus provide critical insights into microbial diversity and metabolic and functional potential, thereby serving as a powerful approach for investigating the impact of bio-mediated processes on nutrient distributions in the ocean (Levine and Leles, 2021). For example, urease was identified as a key enzyme for adaptation to nitrogen-limited environments in the widespread *Thaumarchaeota* (Alonso-Sáez et al., 2012). Similarly, Ni-binding SOD was found to be prevalent in *Synechococcus* strains thriving in Fe-replete waters (Doré et al., 2023), and it is present in all known strains of *Prochlorococcus* and widespread in heterotrophic bacteria and archaea (Sutherland et al., 2021). Metagenomic surveys of hydrogenase diversity across terrestrial and aquatic ecosystems have highlighted hydrogen metabolism as an underestimated energy source for microbial growth (Greening et al., 2016). Comparative genomics and metagenomics have thus highlighted the role of Ni-containing enzymes across a variety of organisms and ecosystems. However, to our knowledge, no study has investigated Ni-containing enzymes distribution in relationship to Ni measurements through large scale metagenomics in the marine environment.

Here, we present Ni concentrations, δ^{60}Ni and metagenomics, all determined from the same stations and depths, in the upper 1000 m of the Atlantic sector of the Southern Ocean and along a transect between Tasmania and Antarctica as part of the Antarctic Circumnavigation Expedition (ACE). The Southern Ocean being a high-latitude environment mainly composed of nutrient-rich waters, we would expect to find heavy Ni isotope compositions only in surface of the lowest latitudes, as based on the hypotheses presented above (Archer et al., 2020; Lemaitre et al., 2022; Bian et al., 2024; Chiu et al., 2026). We provide new data complementing the still limited Ni isotope database in the ocean and aim to provide a clearer picture of where the Ni isotope fractionation occurs between low and high latitudes. Moreover, the high-resolution of the shallow depth profiles enables us to advance our understanding of surface processes driving Ni cycling and therefore to investigate the hypothesis that specific enzymes and microbial communities may play a role in the oceanic Ni biogeochemical divide.

2 Material and methods

2.1 Study area

During the ACE cruise (December 2016–March 2017, R/V *Akademik Tryoshnikov*), seawater samples were collected from the same stations for both Ni concentrations and isotopes (10–12 depths in the upper 1000 m) and for metagenomics (at 5, 15, 150 and 1000 m, complemented by other depths when possible). Sampling was undertaken at 8 stations from Leg 2 (stations 8–11) and Leg 3 (stations 22–25), in the Atlantic and Pacific sectors of the Southern Ocean respectively (Fig. 1). These stations span the major Antarctic Circumpolar Current (ACC) fronts around Antarctica (Orsi et al., 1995): the Sub-Tropical Front (STF), the Sub-Antarctic Front (SAF), the Polar Front (PF), the Southern ACC Front (SACCF) and the Southern Boundary of the ACC (SB). These fronts divide the Southern Ocean into several broadly uniform physical and biogeochemical zones. Macronutrient abundances and phytoplankton communities differ in the surface waters of these frontal zones. Upwelled nutrient-rich waters reach the surface south of the PF, with nutrient concentrations decreasing due to phytoplankton uptake during transport northwards. Intense diatom blooms occur around the PF, depleting silicate in surface waters north of the PF, whereas phosphate and nitrate decrease more gradually until depletion at the SAF (Sarmiento et al., 2004). As a result, meridional changes also occur in phytoplankton communities: diatoms requiring Si for growth are the dominant species as far north as the PF and continue to contribute to the surface communities near the SAF; calcifiers such as coccolithophores play an important role between the SAF and the STF; pico-phytoplankton such as cyanobacteria tend to dominate the phytoplankton community north of the STF (Antoine et al., 2020). Chlorophyll *a* (Chl *a*) concentrations, an indicator of phytoplankton biomass, were generally low along the ACE track ($< 0.5\,\mathrm{mg\,m^{-3}}$; Robinson et al., 2021), which is typical of the high nutrient-low chlorophyll (HNLC) Southern Ocean. However, high Chl *a* was observed in surface waters near shelves, subantarctic islands or in polynya systems near Antarctica (Chl *a* concentrations $= 1.9\,\mathrm{mg\,m^{-3}}$ at station 11, within the Mertz glacier polynya).

2.2 Sample collection and analytical methods for Ni concentrations and isotopes

2.2.1 Seawater sampling

Samples were collected using a trace metal clean rosette equipped with acid-cleaned, Teflon-coated, 10 L X-Niskin bottles, following the recommendations of the GEOTRACES cookbook (Cutter et al., 2017). The rosette was attached to a Dynema line with a dedicated, custom-designed winch, allowing the rosette to be deployed from and landed on the main deck directly outside the trace metal clean container.

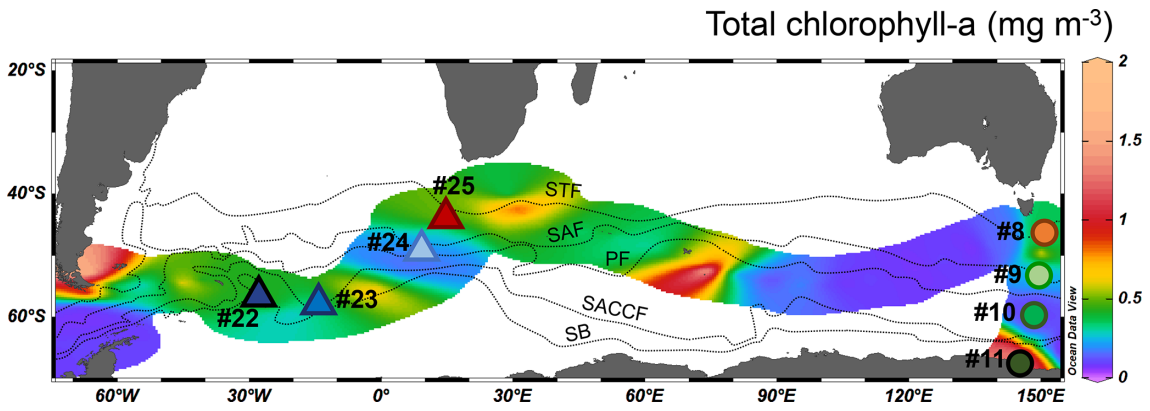

Figure 1. Location of the sampling stations for Ni concentrations, Ni isotopes and metagenomics during the ACE cruise, superimposed on a map of total surface Chlorophyll *a* concentrations from underway seawater samples (Antoine et al., 2020). Blue and green symbols denote high latitude stations, while red and orange symbols represent stations north of the Sub-Antarctic Front from Leg 2 between Tasmania and Antarctica (circle symbols) and from Leg 3 between Patagonia and South Africa (triangle symbols). The major fronts (Orsi et al., 1995) are represented by the dotted black lines: Sub-Tropical Front (STF), Sub-Antarctic Front (SAF), Polar Front (PF), Southern ACC Front (SAAC) and Southern Boundary (SB). The map was generated with ODV (Schlitzer, Reiner, Ocean Data View, odv.awi.de, 2025).

Immediately after recovery, all the Niskin bottles were covered at each end with plastic bags to minimise contamination and were then transferred into the clean container (Class-100) for sampling. Filtered seawater samples for dissolved trace metals were collected by gravity filtration using acid-cleaned 0.2 µm AcroPak cartridge filters (Pall). Between 1 and 4 L of filtrate was collected in acid-cleaned low-density polyethylene (LDPE) bottles and stored at room temperature. Back at the home laboratories at ETH Zurich, the filtered seawater samples were acidified to pH ~ 2 by addition of concentrated hydrochloric acid (HCl; Merck AnalaR grade, further purified by double sub-boiling distillation) and left for at least 3 months before processing. The samples described here have previously been analysed for dissolved Cd, Zn and Fe concentrations and isotopes (Sieber et al., 2019, 2020, 2021).

2.2.2 Dissolved Ni concentration and isotope analyses

All samples were processed at ETH Zurich under clean laboratory conditions (Class 1000) within clean laminar flow hoods (Class 10), using only trace metal clean Savillex PFA labware. All water used was ultrapure ($\geq 18.2\,\mathrm{M\Omega\,cm}$) and all acids and reagents were Merck AnalaR grade, further purified by double sub-boiling distillation.

The methods used here have been previously described and published by the ETH group (Archer et al., 2020; Lemaitre et al., 2022; Wang et al., 2019). Prior to ion exchange purification, a ^{61}Ni-^{62}Ni double-spike was added to reach a sample-to-spike ratio of 1 : 1 and the samples left to equilibrate for 48 h. Samples were then adjusted to pH 5.0 ± 0.3 using an ammonium acetate buffer, before loading onto a preconcentration column containing an ethylenediaminetriacetic acid chelating resin, sold commercially as Nobias PA1 (Hitachi High Technologies; (Sohrin et al., 2008). The seawater matrix was eluted using 30 mmol $\mathrm{L^{-1}}$ ammonium acetate buffer and the metals were extracted from the resin using 1 mol $\mathrm{L^{-1}}$ nitric acid. Trace metals were then separated from each other through an anion exchange column (Bio-Rad AG MP-1M resin). The Ni fraction was further purified using a miniaturised version of the Nobias preconcentration column and a small anion column (to remove any residual matrix cations, Zn or Fe).

Isotope analyses were performed on a Thermo Neptune Plus Multi-Collector-ICPMS operated in low resolution mode at ETH Zurich. Samples were introduced into the mass spectrometer in 0.3 mol $\mathrm{L^{-1}}$ nitric acid via a CPI PFA nebuliser (50 µL $\mathrm{min^{-1}}$) attached to a Cetac Aridus II desolvating nebuliser system, using standard Ni sample and H-skimmer cones. In addition to the Ni isotopes, ^{56}Fe and ^{57}Fe were measured to monitor and correct for potential interference from ^{58}Fe on ^{58}Ni. Mass discrimination was corrected using the double spike, as detailed previously (Cameron and Vance, 2014). Ni stable isotope ratios are all expressed in standard delta notation relative to the primary NIST SRM 986 Ni standard, as follows:

$$\delta^{60}\mathrm{Ni}\,(‰) = \left[\frac{\left(^{60}\mathrm{Ni}/^{58}\mathrm{Ni}\right)_{\mathrm{sample}}}{\left(^{60}\mathrm{Ni}/^{58}\mathrm{Ni}\right)_{\mathrm{NIST\,SRM\,986}}} - 1\right] \times 1000$$

Repeat measurements of secondary standards Nod-A1 and Nod-P1 (USGS Fe-Mn nodules digested and passed through the Ni column chemistry) were used to evaluate the long-term reproducibility of the isotope analyses. Over the course of this and parallel studies, we obtained $\delta^{60}\mathrm{Ni} = 1.04 \pm 0.07‰$ (2 SD, $n = 446$) for NOD-A1 and $\delta^{60}\mathrm{Ni} = 0.34 \pm 0.07‰$ (2 SD, $n = 590$) for NOD-P1. These values are consistent with previously reported values

(Gueguen and Rouxel, 2021). Internal errors of the instrumental analyses, propagated through the double spike algebra, are given in Table S1. The uncertainties on Ni isotope compositions shown in Fig. 2 are either the internal or the long-term error, whichever is larger. Concentrations reported herein were calculated from the double-spike data using the isotope dilution approach.

The ACE Ni concentrations and isotope compositions have been approved by the GEOTRACES Standards and Intercalibration (S&I) committee and have been released in the GEOTRACES IDP2025 (GEOTRACES Intermediate Data Product Group, 2025). Furthermore, the ACE Ni data from the Atlantic sector were compared to those of Archer et al. (2020) and Cameron and Vance (2014) and showed good agreement in the context of variability in other parameters such as phosphate concentrations and temperatures (Fig. S1).

2.3 Analytical methods and clustering techniques for metagenomics

2.3.1 Metagenomics sampling and sequencing protocols

A total of 48 metagenomic samples were collected at the exact stations and depths where Ni measurements were achieved. For each sample, the water was collected from Niskin bottles and filtered into different size fractions: 0.2–3, 0.2–40 and 3–200 µm. Given the small number of 0.2–40 µm samples (6 in this study) and their high genomic similarity with 0.2–3 µm samples (as estimated by SIMKA using all 218 ACE metagenomes; Benoit et al., 2016; Faure et al., 2026a), the 0.2–3 and 0.2–40 µm samples were combined into a small size fraction and treated separately from the large (3–200 µm) size fraction, as in Faure et al. (2026a). The small size fraction is dominated by bacteria and archaea, likely mostly free-living, while the large size fraction is dominated by unicellular eukaryotes, but also contains particle-attached organisms (Faure et al., 2026a). This way, Ni-containing enzymes from phototrophic and heterotrophic bacteria are likely to be found in the small size fraction, while enzymes from eukaryotic micro-algae like diatoms will mostly be limited to the large size fraction. DNA extraction and library preparation was achieved using *Tara Oceans* protocols. Briefly, after filter cryogrinding, DNA was extracted using total RNA/DNA Purification and Nucleospin RNA/DNA Buffer Set (MACHEREY-NAGEL). Metagenomic libraries were prepared using the Illumina kit according to manufacturer instructions. DNA libraries were sequenced on a Novaseq 4000 instrument, with a target of 100M paired-end reads per library (2× 150 bp; 500 bp insert size). The mean number of sequenced paired-end reads across the 48 ACE samples was 142 M.

2.3.2 Selection of gene clusters related to nickel

Different bioinformatic tools were used here for annotating genes with a function (eggNOG which includes PFAM, and KEGG), for annotating contigs with a taxonomy (MMSeqs taxonomy and Kraken) and for clustering genes (CD-Hit and AGNOSTOS clusters). The schematic presented in Fig. S2 summarises the different methods applied to the metagenomic data in this study.

Briefly, short-reads were quality-filtered and assembled by samples using illumina-utils v2.3 (Eren et al., 2013; Minoche approach with default parameters) and MegaHit v1.2.9 (Li et al., 2015; minimum contig length of 1000, meta-sensitive mode). An average of 94.8 % of read pairs passed the filtering step across the 48 ACE samples. Tables summarizing quality-filtering and assembly steps statistics are available from the https://doi.org/10.6084/m9.figshare.29127848.v1 (Faure et al., 2026b). Prodigal v2.6.3 was used to detect Open-Reading Frames (ORFs, i.e. potential protein-coding sequences) in all contigs (Hyatt et al., 2010). For this study we relied on two types of ORFs clusters produced in Faure et al. (2026a): AGNOSTOS gene clusters (AGC), produced through the AGNOSTOS pipeline (Vanni et al., 2022), and unigenes, produced by clustering all ACE ORFs at 95 % similarity and 90 % coverage using CD-Hit (Li and Godzik, 2006). We retrieved the functional annotations of the 89 739 060 unigenes provided in Faure et al. (2026a), based on eggNOG mapper v2.1.0 (Huerta-Cepas et al., 2017) and KOFamScan v1.3.0 (Aramaki et al., 2020). EggNOG and KEGG databases provide complementary functional annotations with different levels of precision. Unigenes of interest for Ni were selected as:

- Unigenes with eggNOG annotations containing one of the words “urease”, “NiFe” or the combination of “superoxide” and “dismutase” (in any of eggNOG-mapper output columns, including narrow orthologous group (OG) description, best OG description and PFAM).

- Unigenes annotated to a KEGG ID corresponding to urease, NiFe hydrogenase or superoxide dismutase (K01427, K01428, K01429, K01430, K03187, K03188, K03189, K03190, K03192, K14048, K00437, K05586, K05587, K05588, K18005, K18006, K18008, K00518, K04564, K04565, K04569, K16627).

All AGC containing at least one ORF belonging to a unigene of interest for Ni were considered of interest for Ni as well. When used, AGC-level eggNOG, PFAM and KEGG annotations are defined as the modal value from the annotations of all cluster’s members. Please note that all types of superoxide dismutase were retrieved in our selection, and we provide results both at the level of the whole enzymatic family (e.g., *Superoxide dismutase* eggNOG description) and focusing more specifically on the Ni-SOD (e.g., *Sod_Ni* PFAM annotation).

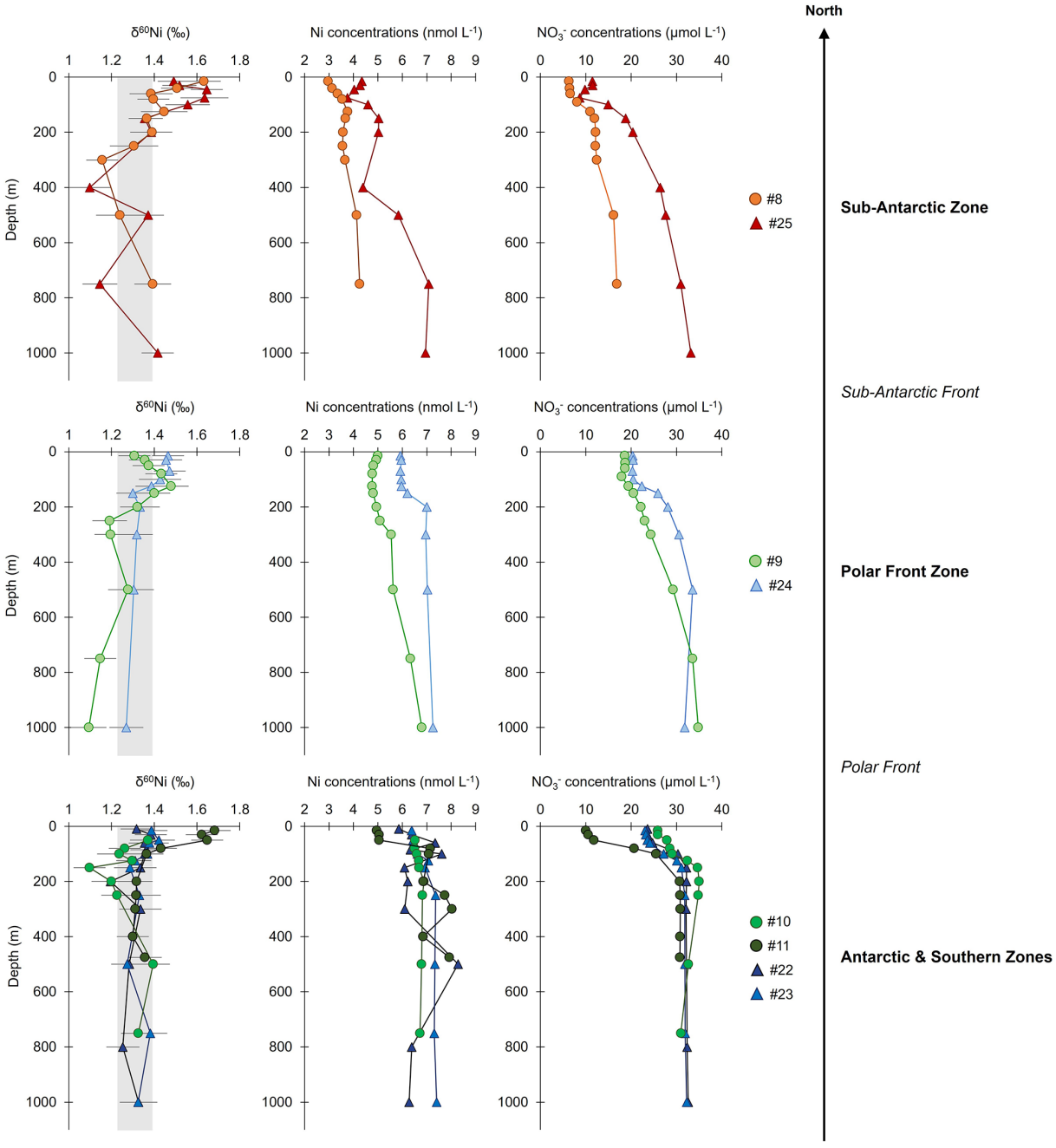

Figure 2. Depth profiles of dissolved Ni isotope compositions (δ^{60}Ni), Ni concentrations and nitrate (NO_3^-) concentrations (from Hassler and Ellwood, 2020) at eight stations of the ACE cruise. The top panels show data from the lower latitudes, in the Sub-Antarctic Zone. Below are panels from the high latitudes, in the Polar Front Zone and in the Antarctic and Southern Zones. The shaded grey band shows the average δ^{60}Ni in the deep ocean (1.34 ± 0.12 ‰, 2SD).

All contigs containing an ORF clustering in a unigene of interest for Ni were taxonomically annotated using MMSeqs2 v14.7e284 with the UniREF90 reference database (Suzek et al., 2015), and Kraken2 (Lu et al., 2022) with the GTDB database (Parks et al., 2022). AGC-level taxonomic annotations were defined as the most frequent in each cluster. Yet, considering the potentially higher taxonomic diversity than functional diversity within cluster, individual ORF annotations were investigated for all clusters of interest (Tables 1, S2).

In addition to Urease, NiFe hydrogenase, and superoxide dismutase, we investigated the potential presence of nitrogen fixation enzymes in our samples but could not show any ev-

idence, suggesting that potential diazotrophs are not present (see Sect. S1.1 and S1.2 in the Supplement).

It should also be noted that our bioinformatic method does not permit the analysis of the presence of eukaryotes in as much detail as bacteria and archaea. Indeed, genes from eukaryotic organisms may comprise coding (exons) and non-coding (introns) DNA sequences, which makes their detection in metagenomic assemblies more difficult than for bacteria and archaea (Stanke et al., 2004). Although there is a significant amount of eukaryotic contigs and genes in the large size fraction (Faure et al., 2026a), our conclusions on the role of eukaryotes in driving Ni isotope fractionation in surface waters of our ACE stations will have to be complemented by genome-resolved and (meta-)transcriptomics studies. Another limitation of our study comes from the significant fraction of uncharacterised sequences due to an absence of matches in current reference databases, estimated to represent 38 % of the ACE reference gene catalog (Faure et al., 2026a). The ACE cruise is the first large-scale metagenomic sampling of the Southern Ocean, and considering the uniqueness of its ecosystem, it is not surprising that a high percentage of unmatched sequences is observed.

2.3.3 Computation and normalisation of function- and cluster-level coverage

Normalised coverages from unigenes and AGNOSTOS gene clusters (AGC) were retrieved in our 48 samples from the abundance matrices computed in Faure et al. (2026a). Briefly, quality-filtered short reads were mapped onto the ACE contig database (i.e., corresponding to all contigs assembled via ACE metagenomes) to produce contigs-level coverage and detection (% of the contigs covered at least at 1X) profiles, using Bowtie v.2.4.5 (Langmead and Salzberg, 2012). Coverage values of all ORFs were extracted using Anvi'o v7.1 (Eren et al., 2015) and summed to obtain unigene- and AGC-level coverages. A threshold of detection was applied to reduce false-positives: all unigene- and AGC-level values of coverage for which no ORF had a detection value of at least 60 % were turned to 0 (see Faure et al., 2026a for justifications). All remaining coverage values were rounded to the nearest integer before normalisation using the relative log expression method from the DeSeq2 R package (Love et al., 2014). To further limit the impact of compositionality and total sample coverage biases, which can impact observed correlations when summing up abundances of large numbers of unigenes (e.g. grouping unigenes by broad functional annotations), we used robust Centered-Log Ratio (r-CLR) and relative transformed abundances computed on all ACE unigenes/AGC. Considering the similarity in the results obtained with the two transformations, we present results based on the easier to interpret relative abundances in Figs. 3 and S3, while equivalent graphs computed on r-CLR transformed data are available in Fig. S4.

Different functional annotation levels were investigated: (1) by summing relative unigene abundances into broad functional groups: urease, NiFe hydrogenase or superoxide dismutase (Fi. S3); (2) by summing relative unigene abundance for each unique functional annotation: KEGG ID, eggNOG best OG description (Fig. 3) or PFAM ID (Fig. 3). Since log-ratio transformations are not additive, we computed the mean of transformed abundances instead of sums when working on r-CLR transformed data (Fig. S4).

2.4 Statistical analyses and metadata collection

All statistical investigations of unigenes/AGC/broad functional groups abundance in relation to Ni measurements were conducted separately on the small and large size fractions. In matrices corresponding to each size fraction, clusters absent in all samples were removed.

Correlations between the various metagenomic coverage values and Ni isotope fractionation were computed using the rank-based Spearman coefficient and tested using a two-sided permutation-based approach (PermCor R package, 1000 permutations). Obtained p-values were adjusted using the Bonferroni-Hochberg correction.

Redundancy analyses (RDA) were achieved on r-CLR-transformed AGNOSTOS gene cluster abundances using the R package vegan v2.6-2 (Oksanen et al., 2022). Only clusters with more than one positive r-CLR-transformed abundance were considered, i.e. 719 AGNOSTOS gene clusters in the small size fraction and 232 AGNOSTOS gene clusters in the large size fraction. The significance of each RDA was tested using the permutations-based test implemented in the anova.cca function.

Considering the role of Ni-containing enzymes in the nitrogen cycle, we decided to investigate the biogeochemical context of our samples regarding nitrogen availability. To do so, we retrieved all available nitrogen-related variables from the ACE metadata compilations. This included concentrations of nitrate, NO_x, ammonium and nitrite, available for all of our samples (Hassler and Ellwood, 2020), as well as the concentration of particulate organic nitrogen (PON) and its associated nitrogen isotope composition ($\delta^{15}N_{PON}$; Fawcett and Forrer, 2020; Stirnimann et al., 2024). We applied a Principal Component Analysis (PCA) on the matrix of Ni and nitrogen variables using the rda function from vegan v2.6-2 (Oksanen et al., 2022). To complement this PCA we further computed individual correlation analysis of the relationship between δ^{60}Ni and PON and nitrate concentrations, again using the rank-based Spearman coefficient and a two-sided permutation-based testing approach.

All scripts necessary to reproduce the statistical analysis achieved in this paper are available at Zenodo: https://doi.org/10.5281/zenodo.21646714 (Faure, 2026).

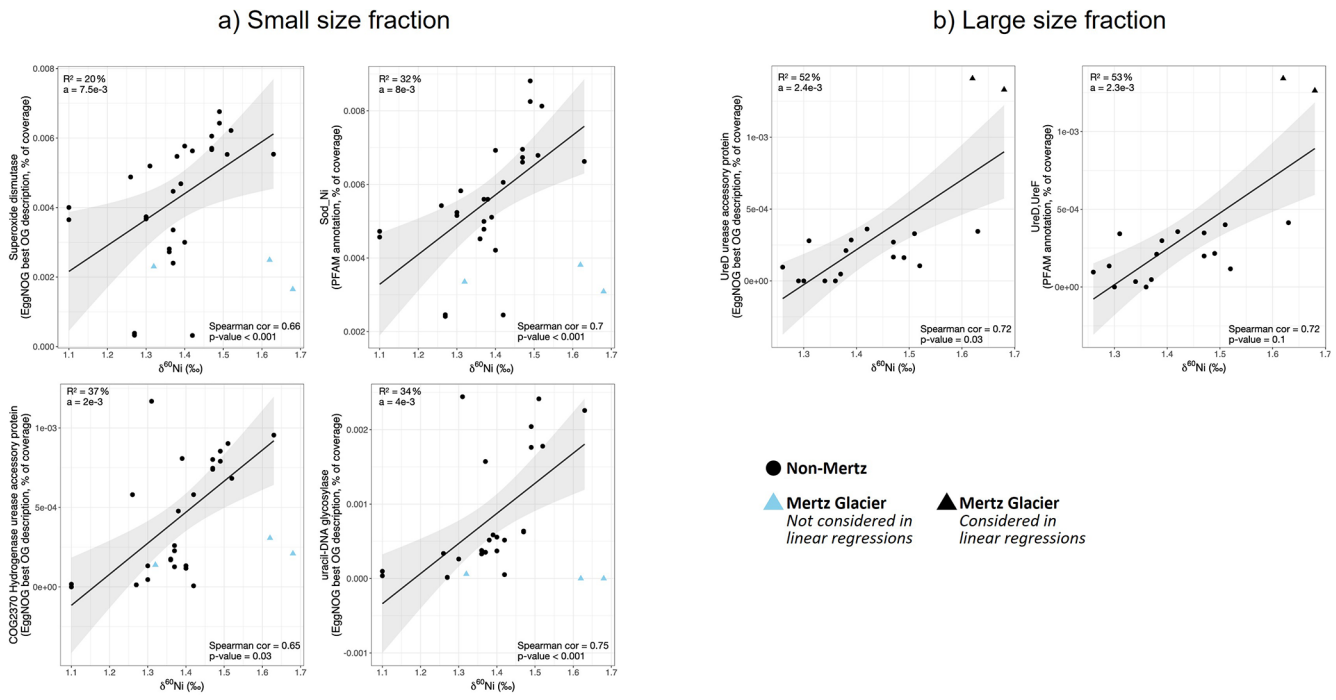

Figure 3. Relative metagenomic abundance (based on EggNOG best OG descriptions or PFAM annotations) as a function of δ^{60}Ni, along with a regression line and its 95 % confidence interval, for **(a)** the small size fraction (0.2–3 and 0.2–40 µm; left panels) and **(b)** the large size fraction (3–200 µm; right panels). Light blue symbols were excluded from the computation of the linear regression lines, to illustrate how removing Mertz Glacier samples from the small size fraction leads to stronger relationships between some functions and δ^{60}Ni. Bonferroni-Hochberg corrected p-values are indicated on each graph (computed without Mertz samples in the small size fraction), along with Spearman coefficients (spearman cor). Adjusted R^2 and slope coefficients (a) of each linear regression are also shown in the top left.

3 Results

3.1 Latitudinal differences in Ni concentrations and isotopes

Dissolved Ni concentrations and isotope compositions for all ACE stations are presented in Fig. 2, and together with macronutrient concentrations and other parameters in Table S1. Overall, dissolved Ni concentrations range from 2.97 to 8.29 nmol L^{-1} and exhibit typical "nutrient-like" profiles, with lower concentrations in surface waters compared to deep. However, there is a strong contrast between the profiles depending on latitude. Only subtle variations are observed with depth at high-latitude stations, south of the Sub-Antarctic Front (stations 9, 10, 22, 23, 24), with only a 1 % median concentration increase between the surface and 100 m. Station 11, near the Mertz Glacier, is an exception among high-latitude stations as it is characterised by a strong decrease of Ni concentrations in the upper 50 m. This pattern is more similar to stations located north of the Sub-Antarctic Front (stations 8 and 25). At these three stations (stations 8, 11, 25), the median concentration increase from the surface to 100 m is 21 %. Stations 8 and 25, north of the Sub-Antarctic Front, have lower surface Ni concentrations (between 3 and 4 nmol L^{-1}) compared to other stations (between 5 and 7 nmol L^{-1}). Depth profiles of nitrate and phosphate concentrations follow similar trends, with lower concentrations in the surface compared to the deep ocean, and with lower surface concentrations at stations north of the Sub-Antarctic Front and at the Mertz Glacier (stations 8, 25 and 11; $\sim$ 10 µmol L^{-1} nitrate and $\sim$ 0.5 µmol L^{-1} phosphate in the upper 50 m) compared to other stations ($\sim$ 20 µmol L^{-1} nitrate and $\sim$ 1.5 µmol L^{-1} phosphate in the upper 50 m).

The overall observed variability in Ni isotope composition is 0.6 ‰, ranging from 1.09 ‰ to 1.68 ‰ for all ACE stations. Similarly to Ni concentrations, variations in δ^{60}Ni throughout the water column are small at high-latitude stations, usually within the range of the average deep ocean value (1.34 $\pm$ 0.12 ‰ at depth > 500 m, mean $\pm$ 2 SD, shaded band in Fig. 2; Cameron and Vance, 2014; Takano et al., 2017; Wang et al., 2019; Archer et al., 2020; Yang et al., 2020, 2021; Lemaitre et al., 2022; Bian et al., 2024; Chiu et al., 2026). Conversely, the Mertz Glacier (station 11) and stations north of the Sub-Antarctic Front (stations 8 and 25) exhibit different depth profiles: as Ni concentrations decrease towards the surface, the isotope composition becomes heavier, with δ^{60}Ni reaching 1.68 ‰, 1.63 ‰, 1.65 ‰ respectively. Such high δ^{60}Ni values have also been observed in surface low-latitude stations in the Atlantic and Pacific oceans

(Takano et al., 2017; Archer et al., 2020; Yang et al., 2020, 2021; Lemaitre et al., 2022; Bian et al., 2024; Chiu et al., 2026). The data reported here thus extend the latitude range of this surface fractionated Ni, in addition to identifying the same signature in a coastal and in a polynya environment.

3.2 Relationship between Ni distributions and metagenomics

The relationships between metagenomics and δ^{60}Ni were studied at various biological precisions, as described below and in Fig. S2: (1) by summing unigenes into broad functional groups, and (2) by investigating AGC, i.e., refined gene clusters that go beyond broad functional annotations.

3.2.1 Urease and superoxide dismutase enzymes associated with heavy Ni isotope composition

In the first approach, we investigated correlations between δ^{60}Ni and relative abundances of unigenes identified as related to the three selected Ni-containing enzymes, comprising 91 unique eggNOG descriptions, 77 unique PFAM annotations and 14 unique KEGG IDs. Sorting abundances into SOD, urease or NiFe hydrogenase functional groups did not lead to significant correlations with δ^{60}Ni, likely because of the strong differences in microbial communities among stations 8, 25 and 11 (Faure et al., 2026a, Fig. S5). However, positive correlations could be observed for SOD in the small size fraction and urease in the large size fraction (Fig. S3).

Looking at individual functional annotations rather than large functional groups, two of the Spearman correlation tests between EggNOG annotations and δ^{60}Ni were significant (Fig. 3). The COG2370 hydrogenase urease accessory protein annotation was significantly correlated to δ^{60}Ni in the small size fraction (adj. p-value $= 0.04$), while the UreD urease accessory protein was significantly correlated to δ^{60}Ni in the large size fraction (adj. p-value $= 0.03$). The COG2370 annotation corresponds to a conserved domain typically involved in the maturation and activation of metalloenzymes requiring Ni as a cofactor, including both NiFe hydrogenase and urease. Station 11 (Mertz polynya) samples drove most of the statistical signal in the large size fraction, while they showed systematically low values of relative abundances in the small size fraction (Fig. 3). Removing Mertz samples from correlation tests, we found 3 additional annotations to be significantly correlated to δ^{60}Ni in the small size fraction (COG2370 correlation remaining significant, adj. p-value $= 0.03$), superoxide dismutase (adj. p-value $< 10^{-3}$), uracil-DNA glycosylase (adj. p-value $< 10^{-3}$) and superoxide dismutase copper chaperone activity (adj. p-value $= 0.04$, likely unrelated or indirectly related to the heavy Ni isotope composition considering its copper-related annotation). Uracil-DNA glycosylase has a role in DNA repair and is not directly linked with Ni. However, the 451 unigenes annotated to Uracil-DNA glycosylase as best OG description in our selection all showed "UreE urease accessory protein, C-terminal domain" as narrow OG description. UreE directly promotes Ni incorporation into urease and shares domain and structure similarities with Uracil-DNA glycosylase: the SMART domain SM00987 (C-terminal domain of UreE) belongs to the structural and functional superfamily of Uracil-DNA glycosylase-like superfamily (SSF52141) and often maps on to the same proteins as SM00986 (Uracil-DNA glycosylase). These similarities may explain the potential confusion in the functional annotation.

In the large size fraction, there are no significant correlations remaining after removing the Mertz samples, and the observed significant correlations do not hold when considering r-CLR transformed data, despite a similar jump in abundance in Mertz samples (Fig. S4). Although correlations between PFAM annotations and δ^{60}Ni were not significant when considering all samples, removing Mertz samples led to two significant correlations in the small size fraction: Sod_Ni (Ni-containing superoxide dismutase; adj. p-value $< 10^{-3}$) and LysE,UDG (Lysine exporter and/or uracil-DNA glycosylase; adj. p-value $= 0.03$, corresponding to unigenes with Uracil-DNA Glycosylase as best OG description, potentially related to UreE as aforementioned). Although insignificant (p-value $= 0.005$, adj. p-value $= 0.1$), the relationship between the UreD,UreF PFAM annotation (activation of urease) and δ^{60}Ni illustrates the positive anomaly in urease abundances at Mertz in the large size fraction. None of the Spearman correlation tests between δ^{60}Ni and KEGG functional annotation-level abundances produced an adjusted p-value below 0.05, thus we do not discuss KEGG KOs below.

3.2.2 Different gene clusters associated with δ^{60}Ni across stations

In the second approach, we investigated the relationship between δ^{60}Ni and individual AGC (i.e., ORFs with similar amino acid sequences), allowing the division of broad functional categories into smaller, more functionally and evolutionarily refined, groups. A total of 1966 AGC were identified as containing at least one ORF annotated as one of the three selected enzymes involving Ni. The RDA were significant for each size fraction (p-values $< 10^{-3}$). In the small size fraction, RDA1 (13.6 % of the variance explained) correlated with δ^{60}Ni, i.e. higher values of δ^{60}Ni were on the positive side of the axis (Fig. 4a). RDA2 (9.1 %) was correlated to Ni concentrations and anti-correlated to δ^{60}Ni. Three AGNOSTOS gene clusters (AGC) were particularly associated with δ^{60}Ni (RDA1 > 0.5 and RDA2 < -0.5). Thirteen AGC were associated with station 11 (RDA1 > 0.5 and $0 >$ RDA2 > -0.5), while 24 AGC were extracted as particularly linked to stations 8 and 25 (RDA2 < -0.5 and $0 <$ RDA1 < 0.5, or RDA2 < 0.75 and RDA1 < 0). In the large size fraction, RDA1 (28.9 %) was positively correlated with Ni concentrations, while RDA2 (8.2 %) was anti-

correlated with δ^{60}Ni (Fig. 4b). AGC_14687886, nearly orthogonal to RDA1 and well projected on the negative side of RDA2, was identified as particularly associated with high δ^{60}Ni (as in the small size fraction). Other AGC located below −0.5 on RDA2 were associated with station 11 when RDA1 > 0, and stations 8 and 25 when RDA1 < 0. Table 1 describes functional and taxonomic annotations of all selected AGC, while a complete description of all extracted clusters is available in Table S2.

3.3 Relationship between Ni distributions and nitrogen availability

The first axis of the PCA achieved on the compilation of Ni and nitrogen variables explained 54.2 % of the variance, and opposed samples with high nitrate, NO_x and Ni concentrations, with samples showing high concentrations of PON, δ^{60}Ni and $\delta^{15}N_{PON}$ (Fig. 5). The correlations between δ^{60}Ni and PON and δ^{60}Ni and nitrates were both significant (p-value = 0.002 and < 0.001, respectively; Fig. S6). This way, all three stations showing heavy Ni isotope compositions share a similar context in terms of nitrogen availability: a strong consumption of nitrate by the phytoplankton has led to high production of organic matter (Stirnimann et al., 2024).

4 Discussion

4.1 Ni concentration and isotope cycling in the Southern Ocean

Overall, the new ACE dataset follows established oceanic Ni-δ^{60}Ni systematics and is consistent with the biogeochemical divide typically reported between low and high latitudes: lower concentrations associated with heavier isotope composition in surface low-latitude waters. The data further refine this divide by demonstrating that Ni fractionation occurs between the Sub-Antarctic and Sub-Tropical Fronts. However, located next to the Mertz glacier, ACE station 11 represents an exception. A decrease in Ni concentrations is accompanied by an increase in δ^{60}Ni in the upper 50 m (Fig. 2), which leads to Ni and δ^{60}Ni systematics at this station that are significantly above the trend described by other high-latitude data (Fig. 6).

At station 11, located within an Antarctic polynya, surface concentrations of macronutrients and other trace metals are also lower than in the surface waters of other high-latitude stations (Janssen et al., 2020; Sieber et al., 2019, 2020, 2021). The lower salinity suggests a meltwater input, but the above authors demonstrated that the resultant dilution of surface seawater cannot explain the lower nutrient concentrations. Instead, they suggest that lower macro- and micronutrient concentrations are due to substantial phytoplankton uptake at station 11, consistent with the high Chl *a* concentrations observed during the cruise (Fig. 1). Sieber et al. (2021) showed that Fe concentrations and isotopes at the Mertz station could be described with a closed-system Rayleigh-type fractionation with an alpha (α) value of 0.999, suggesting that a single process dominates the isotope fractionation. The authors attributed the removal of isotopically light Fe to phytoplankton uptake (Sieber et al., 2021), in line with a significant Fe uptake rate at the same station (Fourquez et al., 2023). Likewise, the clear evolution towards heavy Ni isotope compositions in the upper 100 m of station 11 follows a closed-system Rayleigh fractionation, with $\alpha = 0.99925$ (Fig. 7). Such fractionation cannot be explained by physical mixing. Indeed, surface waters at station 11 consist of upwelled Circumpolar Deep Water (σ_θ CDW ∼ 27.6–27.8 g m^{-3}), whose Ni isotope composition is typical of the average deep world ocean (δ^{60}Ni = 1.31 ‰). This contrasts with the surface of station 11 (δ^{60}Ni > 1.60 ‰), indicating that the isotope fractionation near the surface of station 11 must instead be explained by a local process. To determine whether the isotope fractionation results from biological uptake, phosphate depletion in the water column is compared to Ni depletion in the same samples. At station 11, phosphate and Ni are respectively depleted by 56 % and 31 % between 80 m and the surface. The depletion of both elements is more pronounced than observed at station 10, where phosphate and Ni are only depleted by 4 % and 1 %, respectively. This indicates an enhancement of biological utilisation at station 11 relative to the adjacent station. These observations are further supported by metagenomics investigations of biological diversity within the Mertz polynya compared to the rest of ACE samples (Faure et al., 2026a). Indeed, Mertz samples were very different from all other Sub-Antarctic Surface Water samples, displaying exceptional genomic compositions explained by the abundance of diatoms and a variety of associated heterotrophic bacteria specialized in the use and recycling of organic matter (Faure et al., 2026a).

The fractionation factors at stations 8 and 25, north of the Sub-Antarctic Front, are 0.9988 and 0.99905 respectively, indicating a removal of light Ni isotopes in surface waters, likely due to biological uptake. These fractionation factors are the highest ever reported (Archer et al., 2020; Yang et al., 2021; Bian et al., 2024; Chiu et al., 2026), suggesting that different microbial communities and requirements (e.g., due to Fe limitation) may influence the isotope effect. It is also possible that the systematics between Ni and δ^{60}Ni observed at these two stations may not reflect local processes and could alternatively be due to advection of signatures set elsewhere, as suggested to explain the chromium (Cr) distribution in the ACE samples (Rickli et al., 2019). The shallow samples ($\sigma_\theta < 26.6$ kg m^{-3}) as well as underlying samples ($26.7 < \sigma_\theta < 27.1$ kg m^{-3}) associated with Sub-Antarctic Mode Water originating from the Southern Ocean (σ_θ SAMW ∼ 26.8 kg m^{-3}) are characterised by strong linear relationships between salinity and Ni concentration ($R^2 > 0.82$; Fig. 8a and b), consistent with Rickli et al. (2019). However, unlike for Cr isotopes, the relationships between salinity and δ^{60}Ni for both density intervals are weak

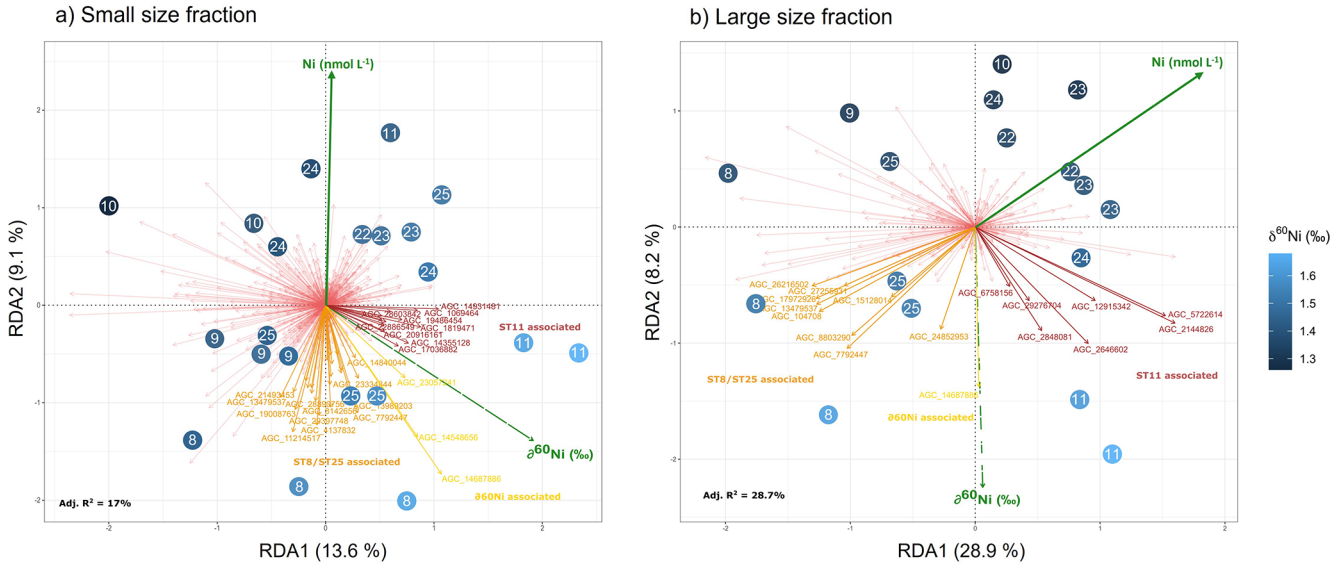

Figure 4. Redundancy analyses (RDA) on the rCLR-transformed abundance of AGNOSTOS gene clusters (AGC) and Ni distributions (concentrations and isotope compositions) for **(a)** the small size fraction (0.2–3 and 0.2–40 µm; on the left side) and **(b)** the large size fraction (3–200 µm; on the right side). Each plain arrow corresponds to a gene cluster. Light red arrows correspond to AGC unrelated to δ^{60}Ni, orange arrows to δ^{60}Ni-related AGC more abundant in stations 8 and 25, yellow arrows to δ^{60}Ni-related AGC well represented in all high-δ^{60}Ni stations, and dark red arrows to δ^{60}Ni-related AGC more abundant at station 11. Each blue dot represents a sample from a specific depth, with the station number shown in white in the middle of the dot, and with the colour indicating the δ^{60}Ni value. Positions of the dots reflect both the enzymatic and Ni/δ^{60}Ni systematics in each sample. Taxonomic and functional annotations of these gene clusters are given in Tables 1 and S2.

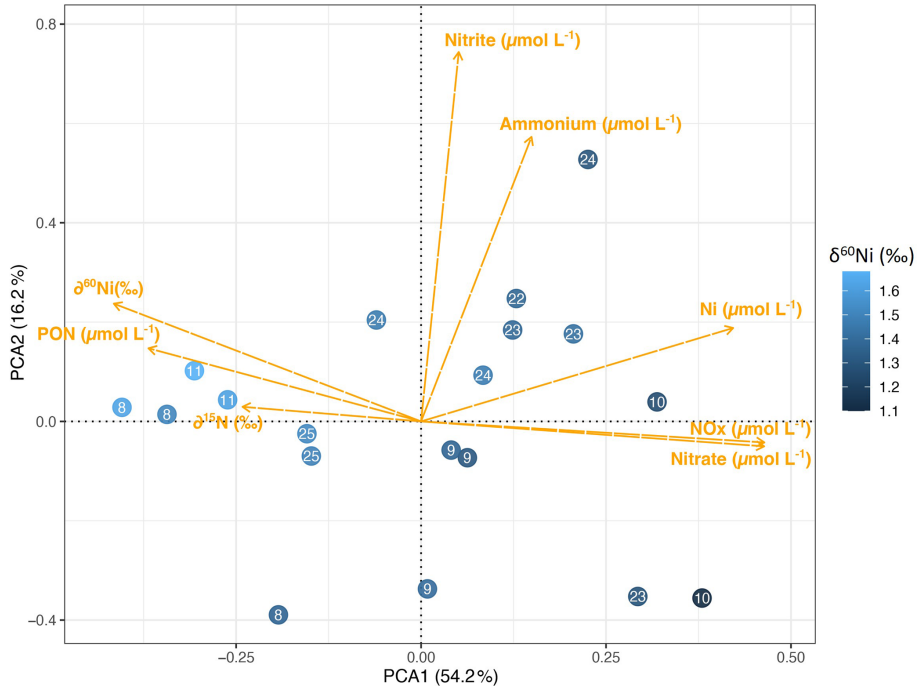

Figure 5. Principal Component Analysis (PCA) on the Ni concentrations and isotopes (δ^{60}Ni) together with inorganic nitrogen concentrations (nitrate, nitrite, ammonium, NO_x), particulate organic nitrogen (PON) concentrations and nitrogen isotope composition from PON (δ^{15}N). Similarly to Fig. 4, each blue dot represents a sample from a specific depth, with the station number shown in white in the middle of the dot, and with the colour indicating the δ^{60}Ni value. Positions of the dots reflect the N-related and Ni-related variables of the different samples.

https://doi.org/10.5194/bg-23-5571-2026

Table 1. Functional and taxonomic annotations of selected AGNOSTOS gene clusters (AGC) emerging from the redundancy analyses as particularly linked to δ^{60}Ni (shown in yellow in Fig. 4), station 11 (shown in red in Fig. 4) and stations 8 and 25 (shown in orange in Fig. 4). The selection of the AGC corresponds to those whose EggNOG best OG description and/or PFAM annotation was clearly related to Ni-dependent enzymes (i.e., not considering non-nickel SOD or ambiguous annotations related to urease like Uracyl-DNA glycosylase). Please, refer to Table S2 for the full functional and taxonomic annotations.

	Size fraction	AGNOSTOS gene cluster	Broad functional annotation	EggNOG based functional annotation	Taxonomic annotation (UniRef90 and GTDB)
δ^{60}Ni	small	AGC_14548656	urease	UreF	Roseobacteraceae, Rhodobacteraceae
	small	AGC_23057241	urease	UreD	Rhodobacteraceae
	small and large	AGC_14687886	urease	UreE_C, UreE_N	Roseobacteraceae, Rhodobacteraceae
Station 11	small	AGC_14355128	Ni-SOD	Sod_Ni	Polaribacter
	small	AGC_20916161	Ni-SOD	Sod_Ni	SAR92
	small	AGC_1069464	urease	UreE_C, UreE_N	Rhodobacteraceae
	large	AGC_2144826	urease	UreD, UreF	Bacillariaceae, Fragilariopsis cylindrus
	large	AGC_29276704	urease	Urease_alpha	Prymnesiaceae, Haptolina ericina
	large	AGC_12915342	urease	cobW, UreG	Naviculaceae, Craspedostauros australis
	large	AGC_6758156	urease	Urease_alpha, Urease_beta, Urease_gamma	Bacillariaceae, Fragilariopsis cylindrus
Stations 8 and 25	small	AGC_23334844	urease	cobW, UreG	Rhodobacteraceae, Roseobacteraceae
	small	AGC_2164110	Ni-SOD	Sod_Ni	Piscirickettsiaceae, Alteromonadaceae, Porticoccaceae
	small	AGC_17472745	NiFe hydrogenase	NiFeSe_Hases	Flavobacteriaceae
	small	AGC_24807388	urease	Urease_alpha, Urease_beta, Urease_gamma	Eukaryote
	small	AGC_8142656	urease	UreE_C, UreE_N	Synechococcus
	small	AGC_25996182	urease	UreD,UreF	Bathycoccaceae
	small	AGC_26196954	Ni-SOD	Sod_Ni	Phaeocystis
	small	AGC_29397748	Ni-SOD	Sod_Ni	Planctomycetaceae, Opitutaceae
	small and large	AGC_13479537	urease	Urease_beta, Urease_gamma	Proteobacteria
	large	AGC_8803290	urease	UreE_C, UreE_N	Rhodobacteraceae, Rhodospirillales, Alteromonadales
	large	AGC_104708	urease	cobW, urease accessory protein	Prasinoderma
	large	AGC_17972926	Ni-SOD	Sod_Ni	Bacillariaceae
	large	AGC_15128014	urease	Urease_alpha, Urease_beta, Urease_gamma	Phaeocystis
	large	AGC_27255931	urease	UreF	Proteobacteria, Synechococcus, Nitrospinae

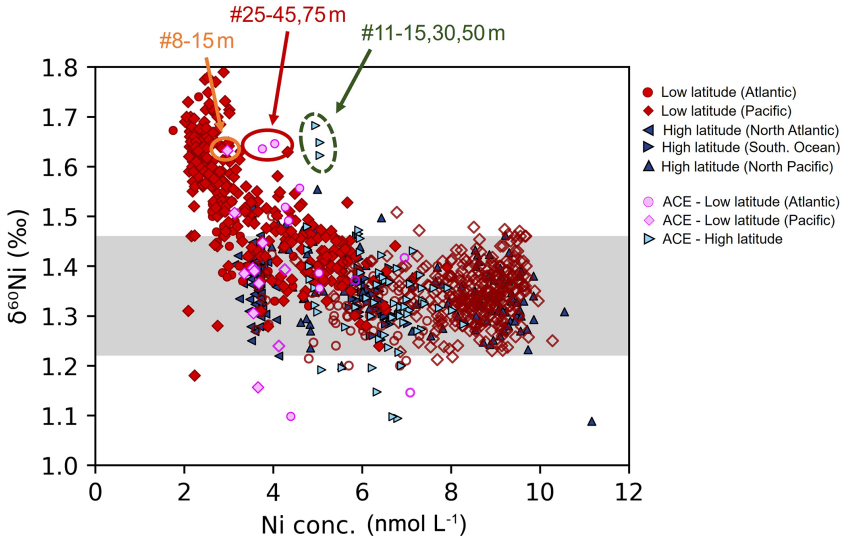

Figure 6. Comparison of the new ACE dataset with the dissolved Ni-δ^{60}Ni systematics of the global ocean (Cameron and Vance, 2014; Takano et al., 2017; Wang et al., 2019; Archer et al., 2020; Yang et al., 2020, 2021; Lemaitre et al., 2022; Bian et al., 2024; Chiu et al., 2026; and this study). The shaded grey band shows the deep-ocean δ^{60}Ni value (see Fig. 2).

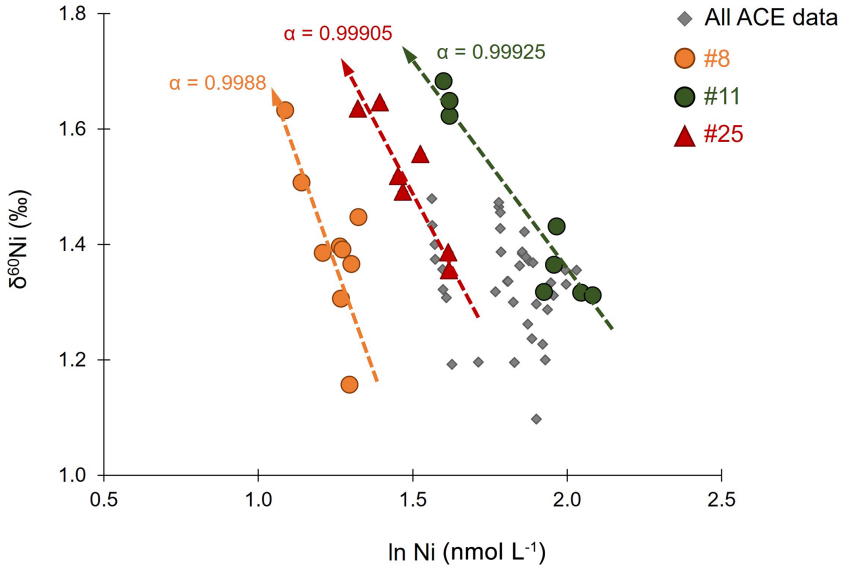

Figure 7. Ni isotope systematics in the upper 300 m of all ACE stations (in grey diamonds), and specifically at stations characterised by significantly heavy isotope compositions in surface waters (station 8 in orange circles, station 11 in dark green circles and station 25 in red triangles). The Rayleigh fractionation factors (α) were calculated using data from the upper 300 m. The arrows show modelled Rayleigh-type evolutions of the residual dissolved phase as Ni is removed from an initial pool ($\delta^{60}Ni_{initial} = 1.31$ ‰) via a generalised uptake mechanism following the equation $R_{residual\ seawater} = R_{initial\ seawater} \times F^{\alpha-1}$, where $\alpha = R_{phytoplankton}/R_{seawater}$, $R = {}^{60}Ni/{}^{58}Ni$ and F is the fraction of the initial pool remaining.

($R^2 < 0.17$; Fig. 8c and d). This suggests that Ni isotope distributions at stations 8 and 25 may not be consistent with conservative mixing. Similarly to station 11, biological uptake may thus be a local process leading to higher δ^{60}Ni values in the surface waters of these northerly stations.

The Ni isotope fractionation in surface waters has been attributed to the biological uptake by cyanobacteria and diazotrophs and was found to correlate with nitrogen fixation in the North Atlantic (Archer et al., 2020; Middag et al., 2020; Lemaitre et al., 2022). But in the present study area, cyanobacteria are scarce (less than 5 % of the phytoplankton stock at stations 8 and 25) or even absent at station 11 (Antoine et al., 2020), and nitrogen fixers are not detected (see Sect. S1.2 in the supplementary information). Nitrogen fix-

ation can therefore not explain the Ni isotope fractionation seen in this study, and the evaluation of other processes is required to explain the Ni distribution patterns observed.

4.2 Metabolic potential in waters with significant Ni isotope fractionation

Faure et al. (2026a) investigated 218 metagenomes across all ACE transects, showing that the Southern Ocean is populated by diverse microbial communities which are largely endemic and structured according to water masses. In addition to characteristics of water masses (temperature, oxygen, salinity and density), they identified the best drivers of microbial composition to be the nitrogen availability (nitrate, NO_x) and presence of diatoms (biological silica, silicic acid). They further highlight the strongly contrasting Mertz polynya (station 11), the only coastal Antarctic ecosystem sampled during the ACE cruise, within Antarctic surface waters. Mertz samples were notably enriched in genes involved in organic matter consumption from species typically associated with polar phytoplankton blooms (e.g., ASP10-02a). It is thus clear that station 11 is distinct from stations 8 and 25 (both in subtropical surface waters) in terms of microbial composition, despite all presenting heavy Ni isotope compositions.

Stations 8 and 25, north of Sub-Antarctic Front, drive the positive correlations observed in the small size fraction between SOD and δ^{60}Ni (only significant when Mertz samples are excluded; Figs. 3a, S4). Similarly, also when Mertz samples are excluded, δ^{60}Ni co-varies with the abundance of two enzymes potentially involved in Ni incorporation in urease: UreE, which is barely distinguished from Uracil-DNA Glycosylase in our annotations, and COG2370, which could also correspond to urease or NiFe hydrogenase. Note that the presence of the NiFe hydrogenase is unlikely, given the absence of statistical signal between NiFe hydrogenase abundance and δ^{60}Ni in all other results. Hence, COG2370 likely corresponds to an accessory protein of urease. The importance of the urease and Ni-SOD enzymes at stations 8 and 25 is confirmed by the RDA analyses of the refined gene clusters (called AGC) in both size fractions (in orange in Fig. 4). The sizes of the Ni-SOD gene clusters in the small size fraction and urease gene clusters in the large size fraction (i.e., the number of unique ORFs they contain) are relatively important, indicating that conserved forms of these genes are frequently found in the ACE metagenomic dataset, suggesting their widespread abundance in the Southern Ocean. The taxonomic annotations of these clusters indicate that the Ni-SOD is carried by diverse heterotrophic bacteria (*Opitutae*, *Planctomycetaceae*, *Piscirickettsiaceae*, *Alteromonadaceae*, *Porticoccaceae*) or by *Phaeocystis*, which is a common phytoplanktonic eukaryote across the Southern Ocean known to use Ni-SOD as an antioxidant (Table 1; Tan et al., 2016). *Porticoccaceae* were identified as the dominant contributors to Fe and Mn transporters in waters above the Kerguelen Plateau, while *Nitrincolaceae*, which were not associated with any of our gene clusters of interest, accounted for most of the signal in Ni transporters, followed by *Rhodobacteraceae* (Kong et al., 2024). The same study identified an Ni-SOD peak during the post-bloom period, without discussing its taxonomic origin (Kong et al., 2024). The urease enzyme is mostly carried by alphaproteobacterial families such as *Rhodobacteraceae* and *Roseobacteraceae* (Tables 1 and S2), matching previous observations from the Arctic (Royo-Llonch et al., 2021; Laso-Pérez et al., 2025). Overall, our results suggest that prokaryotic Ni-SOD and urease enzymes found in the small size-fraction may be involved in Ni consumption and may have contributed to the removal of isotopically light Ni in surface low-latitude waters. However, no specific taxa can explain the isotope fractionation observed at stations 8 and 25.

In contrast of stations 8 and 25, δ^{60}Ni at station 11 seems to be related to large or particle-attached microorganisms, as shown by the significant correlations only observed in the large size fraction. The correlation appears especially strong for the UreD sub-unit, an accessory protein facilitating urease maturation after incorporation of Ni^{2+} inside the cell. The relative abundances of this sub-unit of the urease increase by an order of magnitude compared to other stations (Fig. 3b). The RDA analysis confirms the importance of the urease enzyme at station 11 (in red in Fig. 4), which is carried by the blooming diatoms and associated *Rhodobacteraceae*. A few AGC are annotated as the Ni-SOD enzyme and are carried by *Polaribacter* and *SAR92*, which are heterotrophic bacteria associated with the intense diatom bloom within the Mertz polynya at the sampling time (Tables 1 and S2; Faure et al., 2026a). At this station, the rapid proliferation of heterotrophic bacterial populations (highest total bacteria to Chl *a* ratio at station 11) has been shown to acquire substrates and energy from organic matter (Faure et al., 2026a). In particular, urea has been shown to be an important N source for phytoplankton and prokaryotes near glaciers, where it can account for > 50 % of the total dissolved N (Alonso-Sáez et al., 2012). It is therefore possible that diatoms and *Rhodobacteraceae* have used urea as a nitrogen source, potentially impacting carbon and ammonium availability in a context of high primary productivity (see Sect. 4.3). This potential uptake of urea at station 11 could have led to a greater Ni utilisation through the urease enzyme.

Biological uptake by different microorganisms may thus be responsible for the Ni isotope fractionation, with microorganisms specific of the Southern Ocean at station 11, and more widely distributed microorganisms at stations 8 and 25. This geographical difference in microbial populations bearing Ni-containing enzymes may explain the different fractionation factors – and therefore the different proportions of Ni removed by biological uptake – observed among the three ACE stations with high δ^{60}Ni values in surface waters (Fig. 7). However, there are common findings across gene clusters associated with the three stations, notably recurrent annotations related to the urease enzyme. This led us to in-

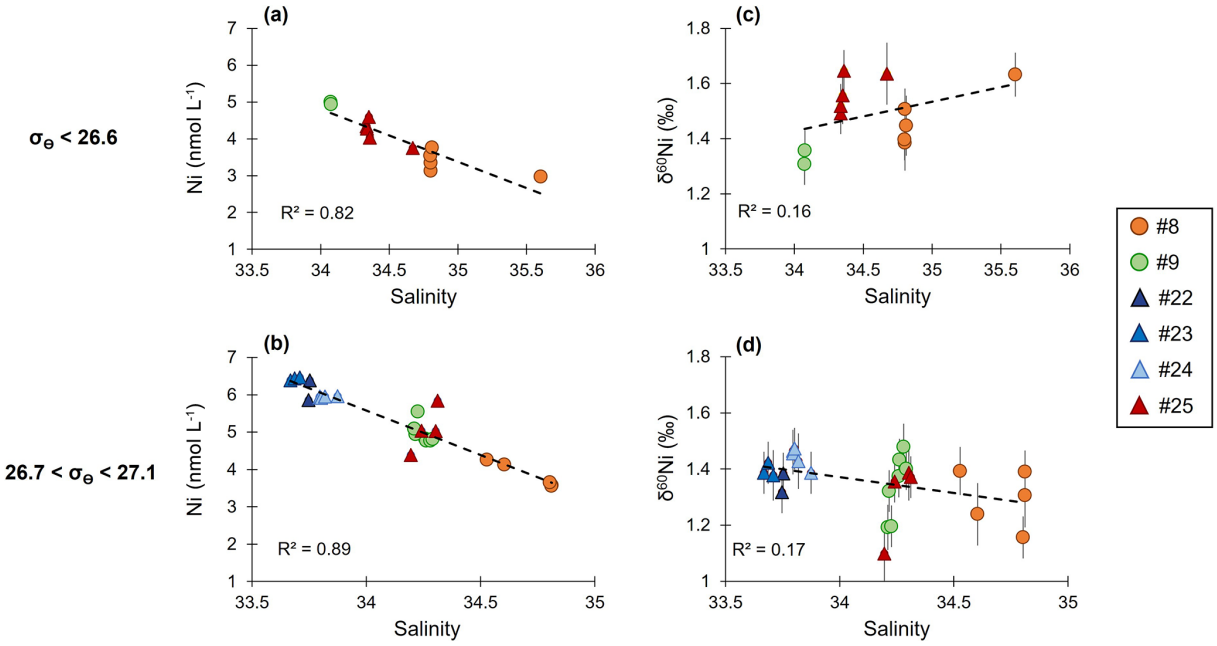

Figure 8. Ni concentrations **(a, b)** and Ni isotopes **(c, d)** versus salinity for surface waters (top panels; $\sigma_\theta < 26.6$) and for waters close to the SAMW isopycnals (bottom panels; $26.7 < \sigma_\theta < 27.1$).

vestigate the potential influence of nitrogen biogeochemistry on the Ni distributions, discussed in the next section.

4.3 Implications for global Ni isotope variability

Stations 8, 25 and 11 are all characterised by the lowest nitrate concentrations ($\leq 10\,\mu mol\,L^{-1}$; Table S1, Fig. 2) and the highest particulate organic nitrogen (PON) concentrations. Interestingly, the organic matter at these 3 stations is also characterised by elevated nitrogen isotope compositions ($\delta^{15}N_{PON}$), consistent with strong nitrate consumption (Fawcett and Forrer, 2020; Stirnimann et al., 2024). We showed that Ni isotope compositions correlate with PON concentrations as well as $\delta^{15}N_{PON}$ and are inversely correlated with nitrate concentrations (Fig. 5). This suggests that enhanced primary productivity at stations with high δ^{60}Ni in surface waters had led to the accumulation of a large PON pool by strongly consuming nitrate. Because microorganisms may face competition for nitrogen acquisition, microbial productivity, particularly bacterial, may thus rely on alternative nitrogen sources, such as urea. This has been observed in Arctic summer blooms, where metatranscriptomics abundance peaks of urease have been detected by multiple studies in the summer blooms (Royo-Llonch et al., 2021; Laso-Pérez et al., 2025). Interestingly, the genomes that dominated the transcription profiles of urease were Alphaproteobacteria and Gammaproteobacteria, matching the annotations of gene clusters directly linked to δ^{60}Ni (in yellow in Fig. 4), which are all annotated as urease enzymes carried by proteobacterial families such as *Rhodobacteraceae* and *Roseobacteraceae*. Furthermore, *Rhodobacteraceae* strains living in interaction with diatoms have been shown to use urease as a nitrogen source in a culture-based study (Zecher et al., 2020). There are also multiple pieces of evidence for the use of urea as a nitrogen source by heterotrophic bacteria in the Arctic winter (Fouilland et al., 2007), and it has been proposed that sea ice could be a source of urea, which could explain the high abundance of urease at Mertz polynya (Conover et al., 1999). This specific nitrogen biogeochemistry in polynya waters could also explain the surprisingly heavy Ni isotope composition at the surface of station 11 compared to other high-latitude stations. In the high latitudes, microbial growth is typically supported by high nitrate concentrations from upwelling or nitrification processes (i.e., oxidation of ammonium to nitrite and nitrate). For example, in waters from the Kerguelen Plateau, nitrification has been shown to supply up to 50 % of the total nitrate uptake in the mixed layer, thereby preventing any nitrogen limitation (Cavagna et al., 2015; Dehairs et al., 2015; Fripiat et al., 2015). Interestingly, no Ni isotope fractionation was observed in these same Kerguelen samples (Wang et al., 2019).

The shift in nitrogen biogeochemistry, together with the observed co-variations between δ^{60}Ni and metagenomics data, may suggest that the Ni isotope fractionation reflects the removal of light Ni by the urease and/or Ni-SOD enzymes, independently of the taxa involved. Considering these results, the biogeochemical Ni divide between low and high latitudes may be driven by Ni metabolic requirements across contrasting regions facing limited nitrogen resource. Further work is required to explore this hypothesis. Measurements of

urea concentration alongside Ni and nitrogen concentrations and isotopes in both dissolved and particulate phases would be beneficial. Extending these analyses to tropical/subtropical waters where cyanobacteria dominate the phytoplankton communities would also be needed, as the dominance of the urease and Ni-SOD enzymes over the NiFe hydrogenase enzyme in the present study may perhaps be explained by the weaker role of this latter enzyme in regions where cyanobacteria and diazotrophs are minor communities. Finally, repeated measurements of δ^{60}Ni and meta-omics data from time-series would help to resolve any potential discrepancies in temporal scales between the datasets. Specifically, while meta-omics captures the instantaneous composition and functional state of microbial communities at the time of sampling, isotope signatures may integrate biological processes over longer periods, spanning days to months.

More investigations are needed to thoroughly define the driver(s) of Ni isotope fractionation in the surface ocean. Elevated δ^{60}Ni in surface waters could reflect the preferential biological uptake of light Ni for enzymatic needs, as proposed in this study and in Lemaitre et al. (2022). Alternatively, elevated δ^{60}Ni could come from a residual, isotopically heavy, non-bioavailable Ni pool due to Ni complexation with organic ligands (between 0 and 2 nmol L^{-1}) assuming negligible isotope fractionation during biological utilisation (Archer et al., 2020). However, at ACE stations with elevated δ^{60}Ni, surface Ni concentrations (2.97 nmol L^{-1} at station 8, 4.95 nmol L^{-1} at station 11 and 4.34 nmol L^{-1} at station 25) exceed the threshold of 2 nmol L^{-1}, arguing against the dominance of the non-bioavailable pool and instead supporting fractionation associated with biological uptake. We nevertheless advocate for further constraints on the bioavailability and isotope composition of the surface organically complexed Ni pool to distinguish these mechanisms.

5 Conclusion and perspectives

This study presents new Ni concentrations, Ni isotope compositions and metagenomics from different frontal zones of the Southern Ocean, using samples from the Antarctic Circumnavigation Expedition (ACE). We aim to explain the patterns observed for both Ni isotope fractionation and enzyme abundances in order to better understand the specific impact of biology on trace metal isotope distributions, information on which is very scarce in the literature. Surface samples at stations north of the Sub-Antarctic Front are characterised by elevated δ^{60}Ni (stations 8 and 25), confirming the Ni biogeochemical divide observed in the world ocean. Peculiar Ni distributions are however observed at the high-latitude station 11, near the Antarctic Mertz glacier: specifically low Ni concentrations associated with high δ^{60}Ni signals, matching low-latitude Ni trends. Our data reveal correlations between enzyme abundance and isotope fractionation, but the strength and significance of these relationships varied with functional databases and stations. These results suggest complex links between enzymes, taxa and Ni isotope fractionation in the ACE samples, with some geographical heterogeneity. The high relative abundance of the urease enzyme in samples from the Mertz Glacier suggests that diatoms and their associated *Rhodobacteraceae* alphaproteobacteria might rely on urea-based nitrogen, thereby consuming Ni and perhaps inducing Ni isotope fractionation. At low-latitude stations, both urease and Ni-SOD, carried by diverse heterotrophic bacteria and phytoplankton species from the small size fraction, are found to correlate with high δ^{60}Ni values.

Therefore, our results suggest that the Ni biogeochemical divide likely reflects the combined activity of multiple microorganisms and enzymatic processes. Interestingly and despite these functional and taxonomic differences, the nitrogen biogeochemistry at these high-δ^{60}Ni stations seems to be in a similar state: nitrates have been strongly consumed and microorganisms, notably bacteria, may rely on alternative sources of nitrogen, such as urea. Understanding the potential biotic and abiotic drivers of the Ni biogeochemical divide will require further research beyond the attempt made here. This should include analyses of urea concentrations in parallel of Ni and nitrogen concentrations and isotopes, a more complete analysis of microorganisms' metabolisms through genome-resolved approaches specifically targeting eukaryotes, and the use of metatranscriptomics to examine the activity of Ni-containing enzymes in addition to their presence. It is also necessary to go beyond correlations by quantifying the impact of enzymatic activity on Ni drawdown and isotope fractionation in controlled lab experiments. Our study identifies different phytoplankton species and heterotrophic bacteria that may all play a role by utilising Ni, as already shown for Fe (Tortell et al., 1996), providing ideal candidate microorganisms and enzymes for future experiments.

Data availability. The new dissolved Ni isotope compositions (δ^{60}Ni) and concentrations, as well as the ACE macronutrient concentrations and CTD data are available in Table S1 and also publicly available through the GEOTRACES intermediate data product 2025 at BODC (https://doi.org/10.5285/42c92148-8d03-8be6-e063-7086abc09f0c, GEOTRACES Intermediate Data Product Group, 2025). Raw metagenomics data are publicly available and can be downloaded from ENA using the accession code ERA30995399. Metagenomic assemblies used in this study are retrievable from Sextant (https://doi.org/10.12770/9c786963-e6a5-4a1c-95f8-1c6ab8a52d2b, Pommellec et al., 2021), while the gene catalogue used in this study is available from Zenodo (https://zenodo.org/records/14181291, Faure et al., 2024). All genomic data specific to nickel-related genes (IDs, contigs of origin, taxonomic and functional annotations), all abundance matrices and environmental metadata used in this study are available from the https://doi.org/10.6084/m9.figshare.29127848.v1 (Faure et al., 2026b), as well as tables summarizing quality-filtering and assembly steps statistics. All scripts necessary to reproduce the statisti-

cal analysis achieved in this manuscript are available at Zenodo (https://doi.org/10.5281/zenodo.21646714, Faure, 2026).

Supplement. The supplement related to this article is available online at https://doi.org/10.5194/bg-23-5571-2026-supplement.

Author contributions. ME, CH, NC, LM planned the campaign. NL, EF, DV and LM co-designed the study. NL, RZ, CA, MS, EF, YL collected samples and/or data. ME, CH, NC, LM, DV and NL acquired fundings. NL and EF wrote the manuscript draft. All co-authors interpreted and discussed the results and contributed to the revision of the manuscript draft.

Competing interests. The contact author has declared that none of the authors has any competing interests.

Disclaimer. Publisher's note: Copernicus Publications remains neutral with regard to jurisdictional claims made in the text, published maps, institutional affiliations, or any other geographical representation in this paper. The authors bear the ultimate responsibility for providing appropriate place names. Views expressed in the text are those of the authors and do not necessarily reflect the views of the publisher.

Acknowledgements. We would like to thank the captain and the crew of the R/V *Akademik Tryoshnikov*, and the chief scientist, the late David Walton for their support at sea. Special thanks go to members of the trace metal clean sampling team including Damien Cabanes, Roger Francois, Marion Fourquez, Samuel Jaccard, Julie Janssen, David Janssen, Maureen Soon and Gregory de Souza. The manuscript was improved by the comments of several anonymous reviewers.

Financial support. This research has been supported by the Swiss National Science Foundation (through the grant 200021_184873), Projects 13 and 15 of the Antarctic Circumnavigation Expedition (funded by EPFL, Swiss Polar Institute and Ferring Pharmaceuticals) and the ANR French Research Foundation ANR-18-CE02-0024 (ACE ecogenomics project). Nolwenn Lemaitre has received funding from the European Union under the Marie Skłodowska-Curie grant agreement 101066172 (Iso-Margin project). Emile Faure has received funding from the European Union under the Marie Skłodowska-Curie grant agreement 101205430 (UNIT-FIX project). Views and opinions expressed are however those of the authors only and do not necessarily reflect those of the European Union or the REA.A – Marie Sklodowska-Curie Actions and Support to Experts. Neither the European Union nor the granting authority can be held responsible for them.

Review statement. This paper was edited by Hermann Bange and reviewed by three anonymous referees.

References

Alonso-Sáez, L., Waller, A. S., Mende, D. R., Bakker, K., Farnelid, H., Yager, P. L., Lovejoy, C., Tremblay, J. É., Potvin, M., Heinrich, F., Estrada, M., Riemann, L., Bork, P., Pedrós-Alió, C., and Bertilssona, S.: Role for urea in nitrification by polar marine Archaea, P. Natl. Acad. Sci. USA, 109, 17989–17994, https://doi.org/10.1073/pnas.1201914109, 2012.

Antoine, D., Thomalla, S., Berliner, D., Little, H., Moutier, W., Olivier-Morgan, A., Robinson, C., Ryan-Keogh, T., and Schuback, N.: Phytoplankton pigment concentrations of seawater sampled during the Antarctic Circumnavigation Expedition (ACE) during the Austral Summer of 2016/2017, Zenodo, https://doi.org/10.5281/ZENODO.3816726, 2020.

Aramaki, T., Blanc-Mathieu, R., Endo, H., Ohkubo, K., Kanehisa, M., Goto, S., and Ogata, H.: KofamKOALA: KEGG Ortholog assignment based on profile HMM and adaptive score threshold, Bioinformatics, 36, 2251–2252, https://doi.org/10.1093/bioinformatics/btz859, 2020.

Archer, C., Vance, D., Milne, A., and Lohan, M. C.: The oceanic biogeochemistry of nickel and its isotopes: New data from the South Atlantic and the Southern Ocean biogeochemical divide, Earth Planet. Sc. Lett., 535, 116118, https://doi.org/10.1016/j.epsl.2020.116118, 2020.

Benoit, G., Peterlongo, P., Mariadassou, M., Drezen, E., Schbath, S., Lavenier, D., and Lemaitre, C.: Multiple comparative metagenomics using multiset k-mer counting, PeerJ Comput. Sci., 2016, 1–25, https://doi.org/10.7717/peerj-cs.94, 2016.

Bian, X., Yang, S. C., Raad, R. J., Odendahl, C. E., Lanning, N. T., Sieber, M., Huang, K. F., Fitzsimmons, J. N., Conway, T. M., and John, S. G.: Distribution and Cycling of Nickel and Nickel Isotopes in the Pacific Ocean, Geophys. Res. Lett., 51, e2024GL111115, https://doi.org/10.1029/2024GL111115, 2024.

Bruland, K. W.: Oceanographic distributions of cadmium, zinc, nickel, and copper in the North Pacific, Earth Planet. Sc. Lett., 47, 176–198, https://doi.org/10.1016/0012-821X(80)90035-7, 1980.

Cameron, V. and Vance, D.: Heavy nickel isotope compositions in rivers and the oceans, Geochim. Cosmochim. Acta, 128, 195–211, https://doi.org/10.1016/j.gca.2013.12.007, 2014.

Cammack, R., Fernandez, V. M., and Hatchikian, E. C.: Nickel-Iron Hydrogenase, Methods Enzymol., 243, 43–68, https://doi.org/10.1016/0076-6879(94)43007-1, 1994.

Cavagna, A. J., Fripiat, F., Elskens, M., Mangion, P., Chirurgien, L., Closset, I., Lasbleiz, M., Florez-Leiva, L., Cardinal, D., Leblanc, K., Fernandez, C., Lefèvre, D., Oriol, L., Blain, S., Quéguiner, B., and Dehairs, F.: Production regime and associated N cycling in the vicinity of Kerguelen Island, Southern Ocean, Biogeosciences, 12, 6515–6528, https://doi.org/10.5194/bg-12-6515-2015, 2015.

Chen, C.-C., Rodriguez, I. B., Chen, Y.-L. L., Zehr, J. P., Chen, Y.-R., Hsu, S.-T. D., Yang, S.-C., and Ho, T.-Y.: Nickel superoxide dismutase protects nitrogen fixation in Trichodesmium, Limnol. Oceanogr. Lett., 7, 363–371, https://doi.org/10.1002/lol2.10263, 2022.

Chiu, C. F., Archer, C., Vance, D., de Souza, G. F., Ellwood, M. J., and Janssen, D. J.: Elucidating the role of biogenic and authigenic phases in marine cycling of nickel with paired dissolved and particulate nickel isotopes, Earth Planet. Sc. Lett., 681, 119934, https://doi.org/10.1016/j.epsl.2026.119934, 2026.

Christians, S. and Kaltwasser, H.: Nickel-content of urease from Bacillus pasteurii, Arch. Microbiol., 145, 51–55, https://doi.org/10.1007/BF00413026, 1986.

Conover, R. J., Mumm, N., Bruecker, P., and MacKenzie, S.: Sources of urea in arctic seas: seasonal fast ice?, Mar. Ecol. Prog. Ser., 179, 55–69, https://doi.org/10.3354/meps179055, 1999.

Cutter, G., Casciotti, K., Croot, P., Geibert, W., Heimbürger, L.-E., Lohan, M., Planquette, H., and Van De Flierdt, T.: Sampling and the sample-handling protocoles for GEOTRACES cruises, 1–178, https://epic.awi.de/id/eprint/51363/1/Cookbook.pdf (last access: 21 July 2023), 2017.

Dehairs, F., Fripiat, F., Cavagna, A. J., Trull, T. W., Fernandez, C., Davies, D., Roukaerts, A., Fonseca Batista, D., Planchon, F., and Elskens, M.: Nitrogen cycling in the Southern Ocean Kerguelen Plateau area: Evidence for significant surface nitrification from nitrate isotopic compositions, Biogeosciences, 12, 1459–1482, https://doi.org/10.5194/bg-12-1459-2015, 2015.

de Vargas, C., Audic, S., Henry, N., Decelle, J., Mahé, F., Logares, R., Lara, E., Berney, C., Le Bescot, N., Probert, I., Carmichael, M., Poulain, J., Romac, S., Colin, S., Aury, J.-M., Bittner, L., Chaffron, S., Dunthorn, M., Engelen, S., Morard, R., Mulot, M., Scalco, E., Siano, R., Vincent, F., Zingone, A., Dimier, C., Picheral, M., Wincker, P., and Karsenti, E.: Eukaryotic plankton diversity in the sunlit ocean, Science, 348, 1–12, https://doi.org/10.1126/science.1261605, 2015.

Doré, H., Guyet, U., Leconte, J., Farrant, G. K., Alric, B., Ratin, M., Ostrowski, M., Ferrieux, M., Brillet-Guéguen, L., Hoebeke, M., Siltanen, J., Le Corguillé, G., Corre, E., Wincker, P., Scanlan, D. J., Eveillard, D., Partensky, F., and Garczarek, L.: Differential global distribution of marine picocyanobacteria gene clusters reveals distinct niche-related adaptive strategies, ISME J., 17, 720–732, https://doi.org/10.1038/s41396-023-01386-0, 2023.

Dupont, C. L., Neupane, K., Shearer, J., and Palenik, B.: Diversity, function and evolution of genes coding for putative Ni-containing superoxide dismutases, Environ. Microbiol., 10, 1831–1843, https://doi.org/10.1111/j.1462-2920.2008.01604.x, 2008a.

Dupont, C. L., Barbeau, K., and Palenik, B.: Ni uptake and limitation in marine Synechococcus strains., Appl. Environ. Microbiol., 74, 23–31, https://doi.org/10.1128/AEM.01007-07, 2008b.

Dupont, C. L., Buck, K. N., Palenik, B., and Barbeau, K.: Nickel utilization in phytoplankton assemblages from contrasting oceanic regimes, Deep-Sea Res. Pt. I, 57, 553–566, https://doi.org/10.1016/j.dsr.2009.12.014, 2010.

Egleston, E. S. and Morel, M. M.: Nickel limitation and zinc toxicity in a urea-grown diatom, Limnol. Oceanogr., 53, 2462–2471, https://doi.org/10.4319/lo.2008.53.6.2462, 2008.

Eren, A. M., Vineis, J. H., Morrison, H. G., and Sogin, M. L.: A Filtering Method to Generate High Quality Short Reads Using Illumina Paired-End Technology, PLoS One, 8, e66643, https://doi.org/10.1371/journal.pone.0066643, 2013.

Eren, A. M., Esen, O. C., Quince, C., Vineis, J. H., Morrison, H. G., Sogin, M. L., and Delmont, T. O.: Anvi'o: An advanced analysis and visualization platformfor 'omics data, PeerJ, 3, 1–29, https://doi.org/10.7717/peerj.1319, 2015.

Faure, E.: EmileFaure/Nickel_Omics, Zenodo [computer software], https://doi.org/10.5281/zenodo.21646714, 2026.

Faure, E., Pommellec, J., Noel, C., Cormier, A., Delpech, L.-M., Eren, M., Fernandez-Guerra, A., Chiara, V., Fourquez, M., Houssais, M.-N., Corinne, D. S., Frederick, G., Perdereau, A., Labadie, K., Guyet, U., Wincker, P., Poulain, J., Hassler, C., Lin, Y., Cassar, N., and Maignien, L.: Southern Ocean Reference Gene Catalogs, Zenodo [data set], https://doi.org/10.5281/zenodo.14181291, 2024.

Faure, E., Pommellec, J., Noel, C., Cormier, A., Delpech, L.-M., Eren, M., Fernandez-Guerra, A., Vanni, C., Fourquez, M., Houssais, M.-N., Da Silva, C., Gavory, F., Perdereau, A., Labadie, K., Wincker, P., Poulain, J., Hassler, C., Lin, Y., Cassar, N., and Maignien, L.: Water mass specific genes dominate the Southern Ocean microbiome, Nat. Commun., 17, 2025, https://doi.org/10.1038/s41467-026-69584-w, 2026a.

Faure, E., Lemaitre, N., Zamora, R., Archer, C., Sieber, M., Ellwood, M. et al.: Biological impacts on the nickel cycle in the Southern Ocean, figshare [data set], https://doi.org/10.6084/m9.figshare.29127848.v1, 2026b.

Fawcett, S. and Forrer, H.: Particulate organic carbon concentration in seawater profiles collected on board the R/V *Akademik Tryoshnikov* in the Southern Ocean during the austral summer of 2016/2017 as part of the Antarctic Circumnavigation Expedition (ACE), Zenodo, https://doi.org/10.5281/zenodo.3706710, 2020.

Fouilland, E., Gosselin, M., Rivkin, R. B., Vasseur, C., and Mostajir, B.: Nitrogen uptake by heterotrophic bacteria and phytoplankton in Arctic surface waters, J. Plankton Res., 29, 369–376, https://doi.org/10.1093/plankt/fbm022, 2007.

Fourquez, M., Janssen, D. J., Conway, T. M., Cabanes, D., Ellwood, M. J., Sieber, M., Trimborn, S., and Hassler, C.: Chasing iron bioavailability in the Southern Ocean: Insights from Phaeocystis antarctica and iron speciation, Sci. Adv., 9, eadf9696, https://doi.org/10.1126/sciadv.adf9696, 2023.

Fripiat, F., Elskens, M., Trull, T. W., Blain, S., Cavagna, A. J., Fernandez, C., Fonseca Batista, D., Planchon, F., Raimbault, P., Roukaerts, A., and Dehairs, F.: Significant mixed layer nitrification in natural iron-fertilized bloom of the Southern Ocean, Global Biogeochem. Cy., 29, https://doi.org/10.1002/2014GB005051, 2015.

GEOTRACES Intermediate Data Product Group: The GEOTRACES Intermediate Data Product 2025 (IDP2025), NERC EDS British Oceanographic Data Centre NOC [data set], https://doi.org/10.5285/42c92148-8d03-8be6-e063-7086abc09f0c, 2025.

Greening, C., Biswas, A., Carere, C. R., Jackson, C. J., Taylor, M. C., Stott, M. B., Cook, G. M., and Morales, S. E.: Genomic and metagenomic surveys of hydrogenase distribution indicate H2 is a widely utilised energy source for microbial growth and survival, ISME J., 10, 761–777, https://doi.org/10.1038/ismej.2015.153, 2016.

Gueguen, B. and Rouxel, O.: The Nickel isotope composition of the authigenic sink and the diagenetic flux in modern oceans, Chem. Geol., 563, 120050, https://doi.org/10.1016/j.chemgeo.2020.120050, 2021.

Guidi, L., Chaffron, S., Bittner, L., Eveillard, D., Larhlimi, A., Roux, S., Darzi, Y., Audic, S., Berline, L., Brum, J. R., Coelho, L. P., Cesar, J., Espinoza, I., Malviya, S., Sunagawa, S., Dimier, C., Kandels-lewis, S., Picheral, M., and Poulain, J.: Plankton networks driving carbon export in the oligotrophic ocean, Nature, 532, 465–470, https://doi.org/10.1038/nature16942, 2016.

Hassler, C. and Ellwood, M.: Nutrient concentration in seawater samples, collected from the underway supply,

CTD and trace metal rosettes in the Southern Ocean during the austral summer of 2016/2017, on board the Antarctic Circumnavigation Expedition (ACE), Zenodo, https://doi.org/10.5281/ZENODO.3923586, 2020.

Ho, T.: Nickel limitation of nitrogen fixation in Trichodesmium, Limnol. Oceanogr., 58, 112–120, https://doi.org/10.4319/lo.2013.58.1.0112, 2013.

Huerta-Cepas, J., Forslund, K., Coelho, L. P., Szklarczyk, D., Jensen, L. J., Von Mering, C., and Bork, P.: Fast genome-wide functional annotation through orthology assignment by eggNOG-mapper, Mol. Biol. Evol., 34, 2115–2122, https://doi.org/10.1093/molbev/msx148, 2017.

Hyatt, D., Chen, G.-L., Locascio, P. F., Land, M. L., Larimer, F. W., and Hauser, L. J.: Prodigal: prokaryotic gene recognition and translation initiation site identification, BMC Bioinformatics, 11, 119, https://doi.org/10.1186/1471-2105-11-119, 2010.

Janssen, D. J., Sieber, M., Ellwood, M. J., Conway, T. M., Barrett, P. M., Chen, X., de Souza, G. F., Hassler, C. S., and Jaccard, S. L.: Trace metal and nutrient dynamics across broad biogeochemical gradients in the Indian and Pacific sectors of the Southern Ocean, Mar. Chem., 221, 103773, https://doi.org/10.1016/j.marchem.2020.103773, 2020.

John, S. G., Kelly, R. L., Bian, X., Fu, F., Smith, M. I., Lanning, N. T., Liang, H., Pasquier, B., Seelen, E. A., Holzer, M., Wasylenki, L., Conway, T. M., Fitzsimmons, J. N., Hutchins, D. A., and Yang, S.: The biogeochemical balance of oceanic nickel cycling, Nat. Geosci., 15, 906–912, https://doi.org/10.1038/s41561-022-01045-7, 2022.

John, S. G., Liang, H., Pasquier, B., Holzer, M., and Silva, S.: Biogeochemical fluxes of nickel in the global oceans inferred from a diagnostic model, Global Biogeochem. Cy., 38, https://doi.org/10.1029/2023GB008018, 2024.

Kong, Y., Zhang, R., Blain, S., and Obernosterer, I.: Seasonal dynamics in microbial trace metals transporters during phytoplankton blooms in the Southern Ocean, Environ. Microbiol., 26, e16695, https://doi.org/10.1111/1462-2920.16695, 2024.

Langmead, B. and Salzberg, S. L.: Fast gapped-read alignment with Bowtie 2, Nat. Methods, 9, 357–359, https://doi.org/10.1038/nmeth.1923, 2012.

Laso-Pérez, R., Rivas-Santisteban, J., Fernandez-Gonzalez, N., Mundy, C. J., Tamames, J., and Pedrós-Alió, C.: Nitrogen cycling during an Arctic bloom: from chemolithotrophy to nitrogen assimilation, mBio, 16, e0074925, https://doi.org/10.1128/mbio.00749-25, 2025.

Lemaitre, N., Du, J., de Souza, G. F., Archer, C., and Vance, D.: The essential bioactive role of nickel in the oceans: Evidence from nickel isotopes, Earth Planet. Sc. Lett., 584, 117513, https://doi.org/10.1016/j.epsl.2022.117513, 2022.

Levine, N. M. and Leles, S. G.: Marine plankton metabolisms revealed, Nat. Microbiol., 6, 147–148, https://doi.org/10.1038/s41564-020-00856-x, 2021.

Li, D., Liu, C. M., Luo, R., Sadakane, K., and Lam, T. W.: MEGAHIT: An ultra-fast single-node solution for large and complex metagenomics assembly via succinct de Bruijn graph, Bioinformatics, 31, 1674–1676, https://doi.org/10.1093/bioinformatics/btv033, 2015.

Li, H., Tuo, S., Lu, M., and Ho, T.: The effects of Ni availability on H2 production and N2 fixation in a model unicellular diazotroph: The expression of hydrogenase and nitrogenase, Limnol. Oceanogr., 9999, 1–11, https://doi.org/10.1002/lno.12151, 2022.

Li, W. and Godzik, A.: Cd-hit: A fast program for clustering and comparing large sets of protein or nucleotide sequences, Bioinformatics, 22, 1658–1659, https://doi.org/10.1093/bioinformatics/btl158, 2006.

Love, M. I., Huber, W., and Anders, S.: Moderated estimation of fold change and dispersion for RNA-seq data with DESeq2, Genome Biol., 15, 1–21, https://doi.org/10.1186/s13059-014-0550-8, 2014.

Lu, J., Rincon, N., Wood, D. E., Breitwieser, F. P., Pockrandt, C., Langmead, B., Salzberg, S. L., and Steinegger, M.: Metagenome analysis using the Kraken software suite, Nat. Protoc., 17, 2815–2839, https://doi.org/10.1038/s41596-022-00738-y, 2022.

Mackey, D. J., O'Sullivan, J. E., Watson, R. J., and Dal Pont, G.: Trace metals in the Western Pacific: temporal and spatial variability in the concentrations of Cd, Cu, Mn and Ni, Deep-Sea. Res. Pt. 1, 49, 2241–2259, https://doi.org/10.1016/S0967-0637(02)00124-3, 2002.

Middag, R., Baar, H. J. W. De, Bruland, K. W., and van Heuven, S. M. A. C.: The distribution of nickel in the west-Atlantic Ocean, its relationship with phosphate and a comparison to cadmium and zinc, Front. Mar. Sci., 7, 1–17, https://doi.org/10.3389/fmars.2020.00105, 2020.

Morel, F. M. M., Lam, P. J., and Saito, M. A.: Trace metal substitution in marine phytoplankton, Annu. Rev. Earth Planet. Sci., 48, 491–517, https://doi.org/10.1146/annurev-earth-053018-060108, 2020.

Oksanen, J., Simpson, G. L., Blanchet, G., Kindt, R., Legendre, P., Minchin, P. R., O'Hara, R. B., Solymos, P., Henrey, M., Stevens, H., Szoecs, E., Wagner, H., Barbour, M., Bedward, M., Bolker, B., Borcard, D., Carvalho, G., Chirico, M., De Caceres, M., Durand, S., Beatriz, H., Evangelista, A., Firtz-John, R., Friendly, M., Furneaux, B., Hannigan, G., Hill, M. O., Lahti, L., McGlinn, D., Ouellette, M.-H., Ribeiro Cunha, E., Smith, T., Stier, A., Ter Braak, C. J. F., and Weedon, J.: vegan: Community Ecology Package, R package version 2.6-2, 2022.

Orsi, A. H., Whitworth III, T., and Nowlin, W. D.: On the meridional extent and fronts of the Antarctic Circumpolar Current, Deep-Sea Res. Pt. I, 42, 641–673, 1995.

Parks, D. H., Chuvochina, M., Rinke, C., Mussig, A. J., Chaumeil, P. A., and Hugenholtz, P.: GTDB: An ongoing census of bacterial and archaeal diversity through a phylogenetically consistent, rank normalized and complete genome-based taxonomy, Nucl. Acids Res., 50, D785–D794, https://doi.org/10.1093/nar/gkab776, 2022.

Pommellec, J., Maignien, L., and Faure, E.: Antarctic Circumnavigation Expedition ecogenomics – METAGENOMES, IFREMER [data set], https://doi.org/10.12770/9c786963-e6a5-4a1c-95f8-1c6ab8a52d2b, 2021.

Price, N. M. and Morel, F. M. M.: Colimitation of phytoplankton growth by nickel and nitrogen, Limnol. Oceanogr., 36, 1071–1077, https://doi.org/10.4319/lo.1991.36.6.1071, 1991.

Ragsdale, S. W.: Nickel-based enzyme systems, J. Biol. Chem., 284, 18571–18575, https://doi.org/10.1074/jbc.R900020200, 2009.

Rickli, J., Janssen, D. J., Hassler, C., Ellwood, M. J., and Jaccard, S. L.: Chromium biogeochemistry and stable isotope distribution in the Southern Ocean, Geochim. Cosmochim. Acta, 262, 188–206, https://doi.org/10.1016/j.gca.2019.07.033, 2019.

Robinson, C. M., Huot, Y., Schuback, N., Ryan-Keogh, T. J., Thomalla, S. J., and Antoine, D.: High latitude Southern Ocean phytoplankton have distinctive bio-optical properties, Opt. Express, 29, 21084–21112, https://doi.org/10.1364/oe.426737, 2021.

Royo-Llonch, M., Sánchez, P., Ruiz-González, C., Salazar, G., Pedrós-Alió, C., Sebastián, M., Labadie, K., Paoli, L., M. Ibarbalz, F., Zinger, L., Churcheward, B., Babin, M., Bork, P., Boss, E., Cochrane, G., de Vargas, C., Gorsky, G., Grimsley, N., Guidi, L., Hingamp, P., Iudicone, D., Jaillon, O., Kandels, S., Not, F., Ogata, H., Pesant, S., Poulton, N., Raes, J., Sardet, C., Speich, S., Setmmann, L., Sullivan, M. B., Chaffron, S., Eveillard, D., Karsenti, E., Sunagawa, S., Wincker, P., Karp-Boss, L., Bowler, C., and Acinas, S. G.: Compendium of 530 metagenome-assembled bacterial and archaeal genomes from the polar Arctic Ocean, Nat. Microbiol., 6, 1561–1574, https://doi.org/10.1038/s41564-021-00979-9, 2021.

Sarmiento, J. L., Gruber, N., Brzezinski, M. A., and Dunne, J. P.: High-latitude controls of thermocline nutrients and low latitude biological productivity, Nature, 427, 56–60, https://doi.org/10.1038/nature10605, 2004.

Sclater, F. R., Boyle, E., and Edmond, J. M.: On the marine geochemistry of nickel, Earth Planet. Sc. Lett., 31, 119–128, https://doi.org/10.1016/0012-821X(76)90103-5, 1976.

Sieber, M., Conway, T. M., de Souza, G. F., Hassler, C. S., Ellwood, M. J., and Vance, D.: High-resolution Cd isotope systematics in multiple zones of the Southern Ocean from the Antarctic Circumnavigation Expedition, Earth Planet. Sc. Lett., 527, 115799, https://doi.org/10.1016/j.epsl.2019.115799, 2019.

Sieber, M., Conway, T. M., de Souza, G. F., Hassler, C. S., Ellwood, M. J., and Vance, D.: Cycling of zinc and its isotopes across multiple zones of the Southern Ocean: Insights from the Antarctic Circumnavigation Expedition, Geochim. Cosmochim. Acta, 268, 310–324, https://doi.org/10.1016/j.gca.2019.09.039, 2020.

Sieber, M., Conway, T. M., de Souza, G. F., Hassler, C. S., Ellwood, M. J., and Vance, D.: Isotopic fingerprinting of biogeochemical processes and iron sources in the iron-limited surface Southern Ocean, Earth Planet. Sc. Lett., 567, 116967, https://doi.org/10.1016/j.epsl.2021.116967, 2021.

Sohrin, Y., Urushihara, S., Nakatsuka, S., Kono, T., Higo, E., Minami, T., Norisuye, K., and Umetani, S.: Multielemental determination of GEOTRACES key trace metals in seawater by ICPMS after preconcentration using an ethylenediaminetriacetic acid chelating resin, Anal. Chem., 80, 6267–6273, https://doi.org/10.1021/ac800500f, 2008.

Stanke, M., Steinkamp, R., Waack, S., and Morgenstern, B.: AUGUSTUS: A web server for gene finding in eukaryotes, Nucl. Acids Res., 32, 309–312, https://doi.org/10.1093/nar/gkh379, 2004.

Stirnimann, L., Bornman, T. G., Forrer, H. J., Mirkin, J., Ryan-Keogh, T. J., Flynn, R. F., Dorrington, R. A., Verheye, H. M., and Fawcett, S. E.: A Circum-Antarctic plankton isoscape: carbon export potential across the summertime Southern Ocean, Global Biogeochem. Cy., 38, e2023GB007808, https://doi.org/10.1029/2023GB007808, 2024.

Sunagawa, S., Coelho, L. P., Chaffron, S., Kultima, J. R., Labadie, K., Salazar, G., Djahanschiri, B., Zeller, G., Mende, D. R., Alberti, A., Cornejo-Castillo, F. M., Costea, P. I., Cruaud, C., D'Ovidio, F., Engelen, S., Ferrera, I., Gasol, J. M., Guidi, L., Hildebrand, F., Kokoszka, F., Lepoivre, C., Lima-Mendez, G., Poulain, J., Poulos, B. T., Royo-Llonch, M., Sarmento, H., Vieira-Silva, S., Dimier, C., Picheral, M., Searson, S., Kandels-Lewis, S., Pesant, S., Speich, S., Stemmann, L., Sullivan, M. B., Weissenbach, J., Wincker, P., Karsenti, E., Raes, J., Acinas, S. G., and Bork, P.: Structure and function of the global ocean microbiome, Science, 348, 1–10, https://doi.org/10.1126/science.1261359, 2015.

Sutherland, K. M., Ward, L. M., Colombero, C. R., and Johnston, D. T.: Inter-domain horizontal gene transfer of nickel-binding superoxide dismutase, Geobiology, 19, 450–459, https://doi.org/10.1111/gbi.12448, 2021.

Suzek, B. E., Wang, Y., Huang, H., McGarvey, P. B., Wu, C. H., and the UniProt Consortium: UniRef clusters: A comprehensive and scalable alternative for improving sequence similarity searches, Bioinformatics, 31, 926–932, https://doi.org/10.1093/bioinformatics/btu739, 2015.

Takano, S., Tanimizu, M., Hirata, T., Shin, K.-C., Fukami, Y., Suzuki, K., and Sohrin, Y.: A simple and rapid method for isotopic analysis of nickel, copper, and zinc in seawater using chelating extraction and anion exchange, Anal. Chim. Acta, 967, 1–11, https://doi.org/10.1016/j.aca.2017.03.010, 2017.

Tan, S., Hu, X., Yin, P., and Zhao, L.: Photosynthetic inhibition and oxidative stress to the toxic Phaeocystis globosa caused by a diketopiperazine isolated from products of algicidal bacterium metabolism, J. Microbiol., 54, 364–375, https://doi.org/10.1007/s12275-016-6012-0, 2016.

Tortell, P., Maldonado, M., and Price, N.: The role of heterotrophic bacteria in iron-limited ocean ecosystems, Nature, 383, 330–332, https://doi.org/10.1038/383330a0, 1996.

Vanni, C., Schechter, M. S., Acinas, S. G., Barberán, A., Buttigieg, P. L., Casamayor, E. O., Delmont, T. O., Duarte, C. M., Eren, A. M., Finn, R. D., Kottmann, R., Mitchell, A., Sanchez, P., Siren, K., Steinegger, M., Glöckner, F. O., and Fernandez-Guerra, A.: Unifying the known and unknown microbial coding sequence space, Elife, 11, 1–60, https://doi.org/10.7554/eLife.67667, 2022.

Vernette, C., Lecubin, J., Sánchez, P., Acinas, S. G., Babin, M., Bork, P., Boss, E., Bowler, C., Cochrane, G., De Vargas, C., Gorsky, G., Guidi, L., Grimsley, N., Hingamp1, P., Iudicone, D., Jaillon, O., Kandels-Lewis, S., Karp-Boss, L., Karsenti, E., Not, F., Ogata, H., Poulton, N., Pesant, S., Sardet, C., Speich, S., Stemmann, L., Sullivan, M. B., Sunagawa, S., Wincker, P., Sunagawa, S., Delmont, T. O., Pelletier, E., Pelletier, E., Hingamp, P., and Lescot, M.: The Ocean Gene Atlas v2.0: online exploration of the biogeography and phylogeny of plankton genes, Nucl. Acids Res., 50, W516–W526, https://doi.org/10.1093/nar/gkac420, 2022.

Wang, R. M., Archer, C., Bowie, A. R., and Vance, D.: Zinc and nickel isotopes in seawater from the Indian Sector of the Southern Ocean: The impact of natural iron fertilization versus Southern Ocean hydrography and biogeochemistry, Chem. Geol., 511, 452–464, https://doi.org/10.1016/j.chemgeo.2018.09.010, 2019.

White, R. A., Callister, S. J., Moore, R. J., Baker, E. S., and Jansson, J. K.: The past, present and future of microbiome analyses, Nat. Protocols, 11, 2049–2053, https://doi.org/10.1038/nprot.2016.148, 2016.

Yang, S., Kelly, R. L., Bian, X., Conway, T. M., Huang, K., Ho, T., Neibauer, J. A., Keil, R. G., Moffett, J. W., and John, S. G.: Lack

of redox cycling for nickel in the water column of the Eastern tropical north pacific oxygen deficient zone: Insight from dissolved and particulate nickel isotopes, Geochim. Cosmochim. Acta, 309, 235–250, https://doi.org/10.1016/j.gca.2021.07.004, 2021.

Yang, S. C., Hawco, N. J., Pinedo-González, P., Bian, X., Huang, K.-F., Zhang, R., and John, S. G.: A new purification method for Ni and Cu stable isotopes in seawater provides evidence for widespread Ni isotope fractionation by phytoplankton in the North Pacific, Chem. Geol., 547, 119662, https://doi.org/10.1016/j.chemgeo.2020.119662, 2020.

Youn, H.-D., Kim, E.-J., Roe, J.-H., Hah, Y. C., and Kang, S.-O.: A novel nickel-containing superoxide dismutase from Streptomyces spp, Biochem. J., 318, 889–896, https://doi.org/10.1042/bj3180889, 1996.

Zecher, K., Hayes, K. R., and Philipp, B.: Evidence of interdomain ammonium cross-feeding from methylamine- and glycine betaine-degrading Rhodobacteraceae to Diatoms as a widespread Interaction in the Marine phycosphere, Front. Microbiol., 11, 1–15, https://doi.org/10.3389/fmicb.2020.533894, 2020.